Responses to RC1:

General comments:

This manuscript applies multiple linear regression (MLR) to monthly mean zonal wind data in the stratosphere, mesosphere, and lower thermosphere obtained from SABER observations, MF and meteor radar observations, and MERRA2 meteorological reanalysis to examine the effects of QBO, ENSO, and solar activity as well as seasonal changes and long-term trends. Although many similar studies based on the MLR analyses have been conducted using long-term meteorological reanalysis data, there have been few research above the stratopause due to the difficulty of observing winds. In this sense, the efforts in this manuscript are commendable. On the other hand, the method of MLR analysis and statistical significance are not well documented, and the consideration of the short data period is not sufficient. In addition, English grammar check by a native speaker is also recommended. Therefore, I think that this manuscript needs substantial revision before publication. Detailed comments are given below.

Response: Thanks for your valuable comments on our manuscript. The main improvements in this version are:

(1) To elucidate the MLR model better and to remove the collinearity of predictors, the seasonal variations and the responses of winds to F10.7, QBO_{30} (QBOA), QBO_{10} (QBOB), and MEI are retrieved through three steps. Each step has specific purpose and formulae. We note that although the procedures of applying MLR is changed from that in the last version, this does not change the main results and conclusions significantly.

(2) The statistical significance is estimated by p-value, which is used to replace the standard deviation in the last version.

(3) We applied the new MLR procedure to the 40 years of MERRA2 data (MerU40) and compared with the 18 years of MERRA2 data (MerU18). Below ~55 km, the consistencies of the responses of MerU18 and MerU40 to QBOA and ENSO are better than those to F10.7 and the linear variations. Moreover, at ~40 km and above the equator, the significant negative linear variations of MerU40 coincide well with those MerU18.

(4) The impacts of major SSWs (2003, 2005, 2006, 2007, 2009, 2010, 2013, 2018, 2019) on the trend and responses have been checked in winter months (December, January, February) and in the annual mean. Here the SSW events are adopted from Chemical Sciences Laboratory of NOAA (https://csl.noaa.gov/groups/csl8/sswcompendium/majorevents.html).

(5) English grammar is improved.

Please see the point-to-point responses below.

Major comments:

1. Time interval of the data: It seems that 18 years are too short to fit the 11-year solar cycle. Although the authors evaluated its impacts by changing the time interval, half or more of the data periods overlap, which does not seem very meaningful. Rather, a comparison using 40 years of MERRA2 data would be more meaningful. As the authors say, the MLS has been assimilated since 2004, but its effect appears to be strong only for the vertical structure of temperature, not so much for the meridional gradient of temperature and the distribution of zonal wind that is related to the meridional gradient of temperature.

Response: Following your suggestion, we have performed the new MLR procedure (see details in Respons#2 and in the text) on the 40 years (1980–2019) of MERRA2 data (MerU40). The monthly zonal mean wind at 25°S and 50 km is taken as an example to show the de-seasonalized results (Fig. R1) and MLR results (Fig. R2).

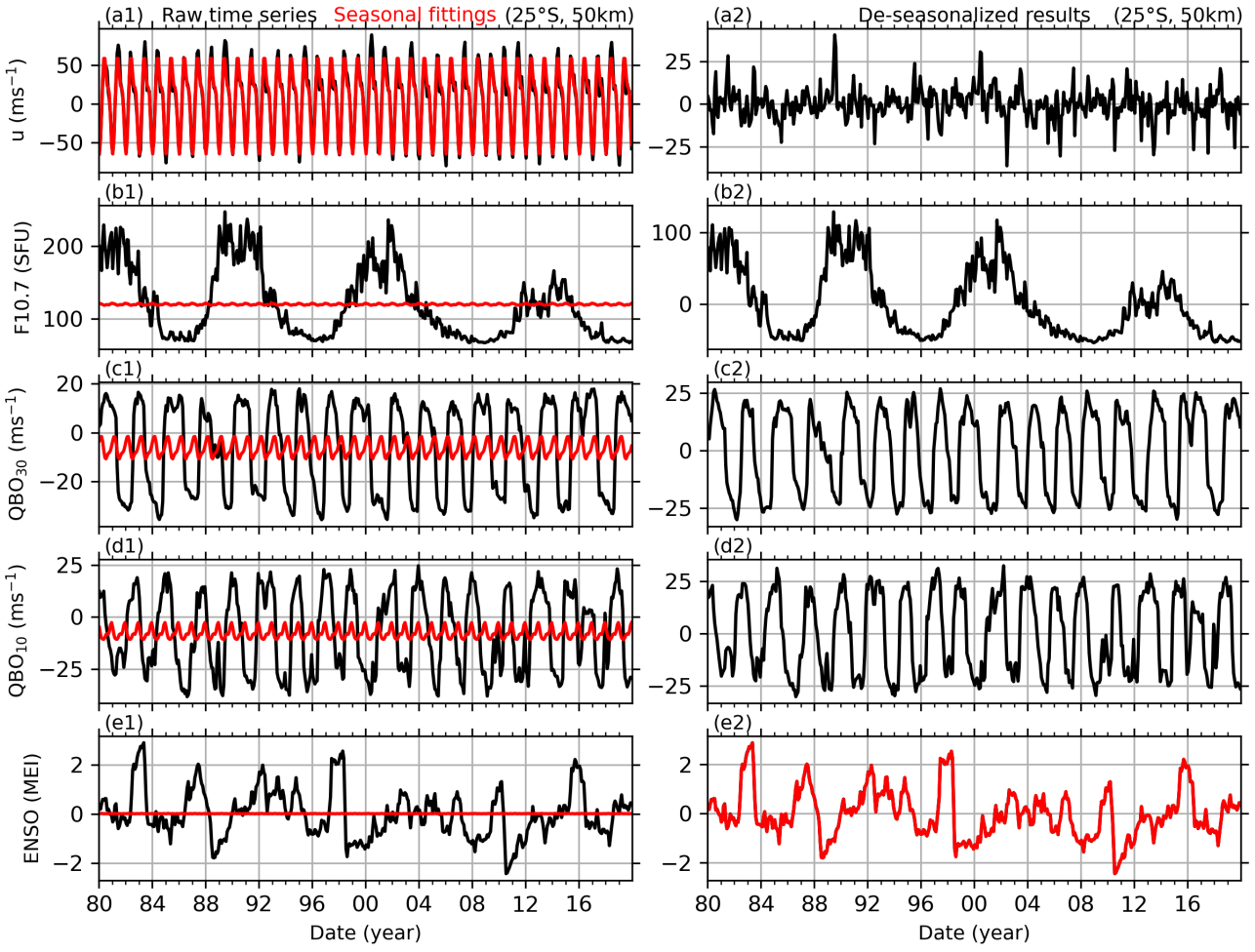

Figure R1: Example of the reference time series (left column) and their de-seasonalized results (right column). The first row: BU at 25°S and 50 km (black line in a1) and its seasonal fitting result (red line in a1), and the residual of BU (black line in a2). The second, third, and fourth rows: same captions as the first row but for solar activity (indicated by F10.7), QBO at 30 hPa (QBO_{30} or QBOA) and at 10 hPa (QBO_{10} or QBOB), and ENSO (indicated by MEI index). The red line in e2

is the residual of MEI index after removing the response of MEI to F10.7.

Figure R1 shows that the seasonal variations are important in the wind (Fig. R1a1 and a2) but are insignificant in the time series of F10.7, QBO_{30} (QBOA) , QBO_{10} (QBOB), and ENSO (Fig. R1b1-e2). Figure R2a1 shows that the responses of MerU40 to F10.7 are significant (p-value ≤ 0.1) in March, April, and August. This is different from the responses of the 18-year data (short for MerU18) to F10.7, which are significant only in May. The responses of MerU40 to QBOA and QBOB (Fig. R2b1) are significant in April–June and in October. This is similar to those of MerU18, which are also significant in May–June, but insignificant in April and October. The responses of MerU40 to ENSO (Fig. R2c1) are negative and significant in January–April and December. However, the responses of MerU18 to ENSO are also negative but are insignificant. The linear variations of MerU40 (Fig. R2d1) are significant in March and April (positive values) and in November and December (negative values). However, the responses of MerU18 are insignificant (judged by p-value > 0.1) in all months.

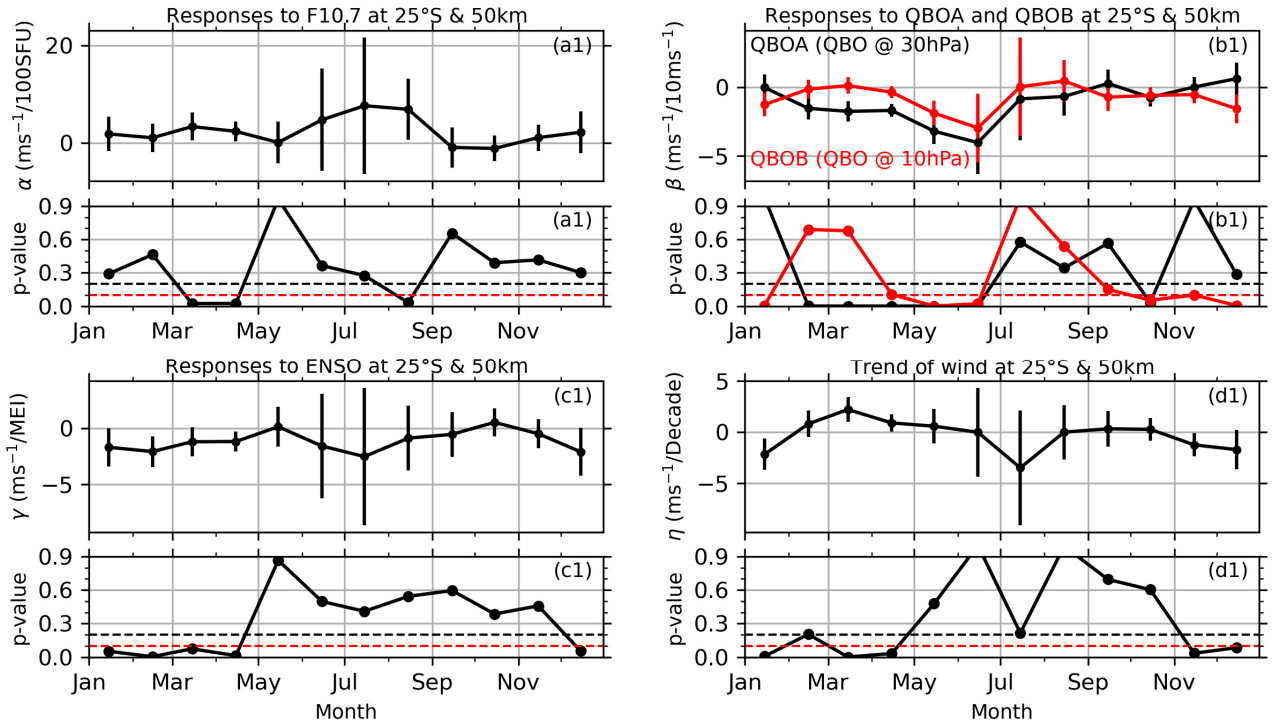

Figure R2: Example of retrieving the monthly responses of MerU40 at 25°S and 50 km (upper subplot of each panel) and their p-values (lower subplot of each panel) to solar activity (a1 and a2) QBOA (black in b1 and b2) and QBOB (red in b1 and b2), ENSO (c1 and c2), and the linear variations (d1 and d2). The error bars are the confidence interval at 90% confidence level. The red and black dashed lines indicate the p-values of 0.1 and 0.2, respectively.

Figure R3 shows the seasonal variations of MerU40 (upper row) and the responses of MerU40 (middle row) and MerU18 (lower row) to various predictors. We see that AO, SAO, and TAO of

MerU40 exhibit similar latitude-height distributions as those of the MerU18. The responses of MerU40 to QBOA are similar to those of MerU18 on the aspects of magnitudes and patterns but have a wider significant region around the equator. Around the equatorial region, the responses of MerU40 to ENSO have similar patterns to those of MerU18 around the equatorial region. However, the positive responses of MerU40 to ENSO are stronger (weaker) than those of MerU18 below ~30 km (around ~40–45 km). Around ~20°S and above ~55 km, the negative responses of MerU18 to ENSO are stronger than those of MerU40. At ~40°S and around ~30 km, the significant positive responses of MerU18 to ENSO cannot be seen in those of MerU40. The significant responses of MerU18 to F10.7 occur in wider height ranges as compared to those of MerU40 around the equator. Moreover, at latitudes higher than 30°S, the responses of MerU18 to F10.7 are negative as compared to the positive responses of MerU40 to F10.7. At around 40°N and ~40–60 km, the positive responses of MerU18 to F10.7 are weaker and less significant than those of MerU40. The linear variations of MerU18 coincide with those of MerU40 above ~30 km, except around ~45°N/S, where the negative linear variations of MerU40 (MerU18) are significant (insignificant). Below ~30 km, the positive linear variations of MerU40 extend to wider latitudes as compared to those of MerU18.

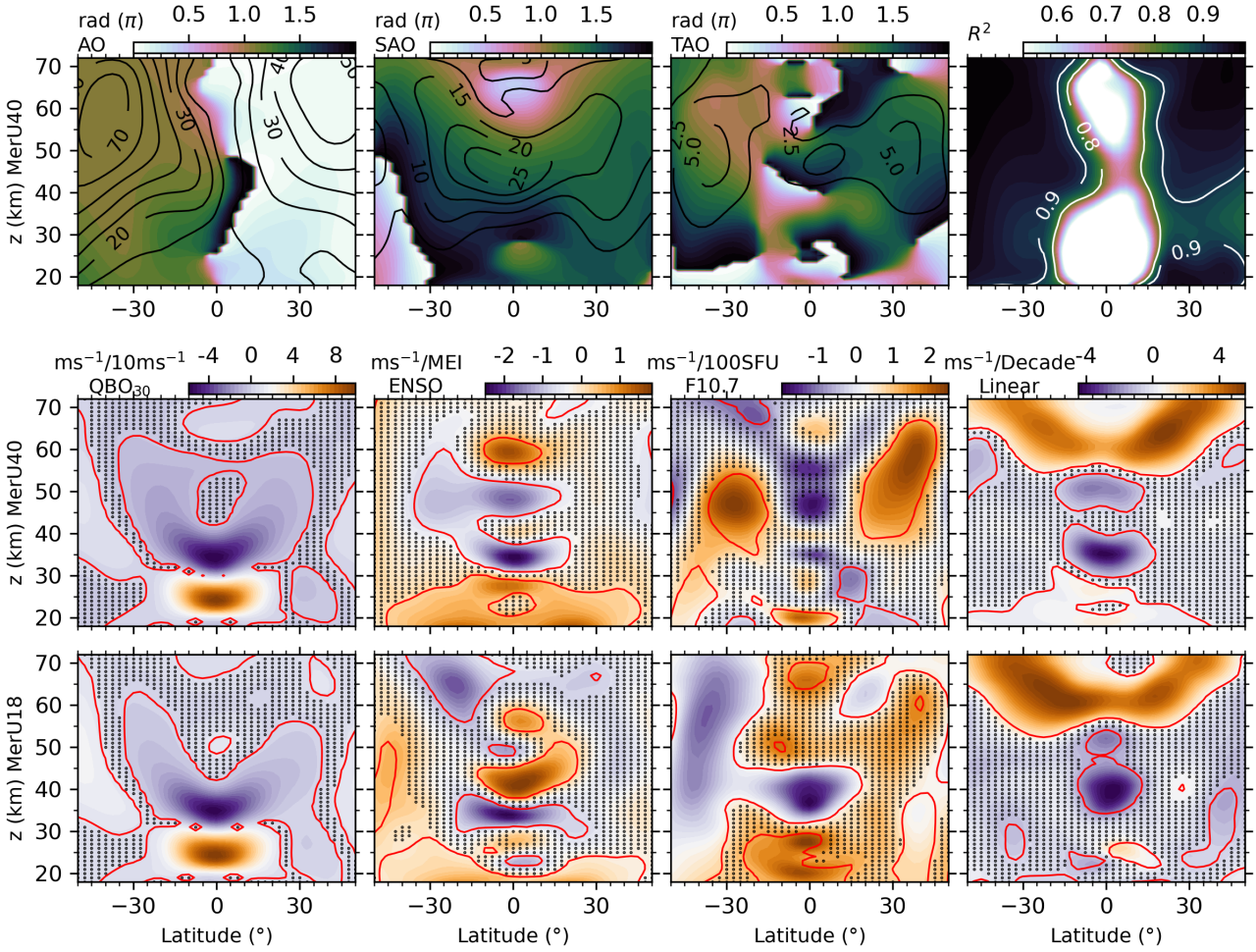

Figure R3: Upper row: the latitude-height distributions of the amplitudes (contour lines) and

phases (color scale) of seasonal variations and the R^2 scores (from left to right) of MerU40. Middle row: the latitude-height distributions of the responses of MerU40 to QBOA, ENSO, F10.7 and linear variations (from left to right). Lower row: same caption as the middle row but for the MerU18. The black dots indicate that the regression coefficients with p-values larger than 0.2. The red lines indicate the regression coefficients with p-values of 0.1.

A summary of the responses and linear variations of MerU18 and MerU40 below ~55 km (this is most reliable height since the damping is significant above this height (Ern et al., 2021)) is below. **The consistencies of the responses of MerU18 and MerU40 to QBOA and ENSO are better than those to F10.7 and the linear variations. Moreover, at ~40 km and around the equator, the significant negative linear variations of MerU40 coincide well with those MerU18.**

2. Method of MLR analysis: From the explanation in section 2.2, it appears that eq. (2) is applied to data for 216 months over 18 years, in which case only one regression coefficient is obtained for the entire period. On the other hand, section 3 shows that regression coefficients were obtained for each month, suggesting that eq. (2) without including the seasonal variation term was actually applied to 18 years of data for each month. In that case, I do not know how the seasonal variation was estimated. The authors need to properly explain the MLR method.

Response: You are right. In the last version, the regression model is,

$$u(t_i) = A_0 + \text{Season}(t_i) + \alpha \text{F10.7}(t_i) + \beta_{30}\text{QBO}_{30}(t_i) + \beta_{10}\text{QBO}_{10}(t_i) + \gamma \text{ENSO}(t_i) + \eta t_i + \text{Res}(t_i). \quad \text{(R1)}$$

Equation R1 is applied to data for 18 years. Moreover, the regression coefficients $\alpha, \beta_{30}, \beta_{10}, \gamma, \eta$ are not specific numbers but depend on the month. They have the form of (for example, α):

$$\alpha = \alpha_0 + \sum_{k=1}^{3}[\alpha_{2k-1}\cos(k\omega t_i) + \alpha_{2k}\sin(k\omega t_i)]. \quad \text{(R2)}$$

Here, $\omega = 2\pi/12$ (month). The regression coefficient of F10.7 in January is obtained by setting $t_i = 1$ in Eq. R2. In a same way, the regression coefficient in February can be obtained by setting $t_i = 2$ in Eq. R2, and so on. Then we can get the regression coefficients in 12 months. The annual mean regression coefficient is obtained by averaging the regression coefficients in 12 months. Moreover, Eq. R1 and R2 play a role of de-seasonalizing regressor and predictors. This method was proposed by Randel and Cobb (1994) (Eq. 1 and 2 of their paper) and other researchers due to its highly compactable and portable in applications.

In this version, to easily explain the MLR model and to remove the collinearity of predictors, the seasonal variations and the responses of wind to F10.7, QBOA, QBOB, and MEI are retrieved through three steps. Each step has specific purpose and formulae. The detailed revision has been made in the text:

The detailed applications of MLR to retrieve the seasonal variations of winds and the responses of winds to F10.7, QBOA, QBOB, and MEI can be ascribed to the following three steps. For illustrative purpose, BU at 25°S and 50 km (black in Fig. R4a1) is taken as an example to show the procedure of MLR. This procedure is also applied to winds at other latitudes and heights, but results in different regressions coefficients due to the latitudinal and height dependencies of the seasonal variations and the responses of winds to F10.7, QBOA, QBOB, and MEI.

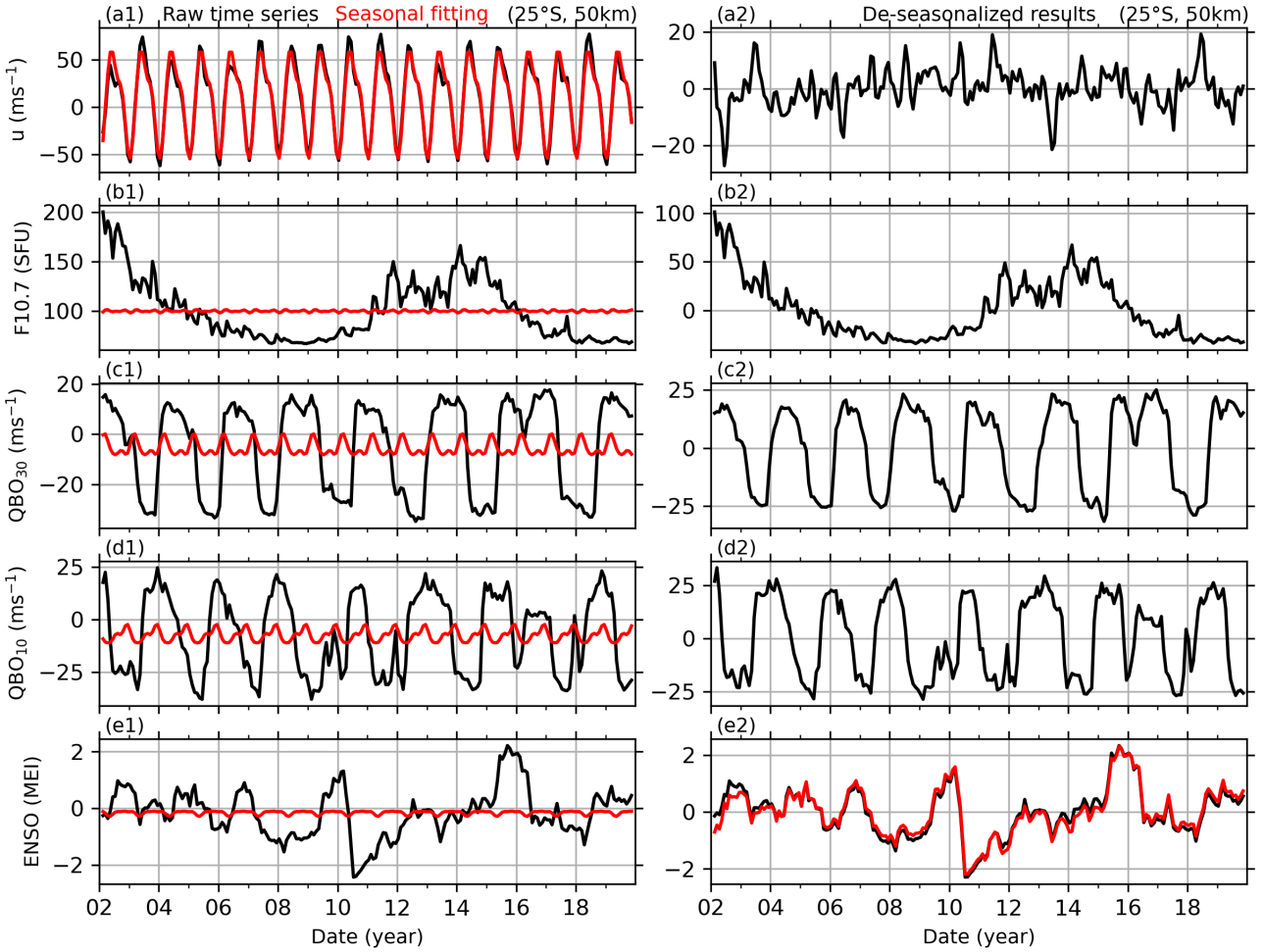

Figure R4: Same caption as Fig. R1 but for the BU at 25°S and 50 km during 2002–2019.

First, we de-seasonalize the wind and reference time series by fitting the following harmonics through the least squares method. At each latitude and height, the wind series is fitted as,

$$u(t_i) = u_0 + \sum_{k=1}^{3} A_k \cos[k\omega(t_i - \varphi_k)] + u_{res}(t_i). \quad \text{(R3)}$$

Here, t_i $(i = 1, 2 \cdots, N)$ is the month number since February 2002. u_0 is the mean wind in the entire temporal interval, u_{res} is the de-seasonalized wind. $\omega = 2\pi/12$ (month), A_k and φ_k are the amplitude and phase of the annual (AO, $k = 1$), semiannual (SAO, $k = 2$), and terannual (TAO, $k = 3$) oscillations, respectively. In the same way, Eq. R3 is used to de-seasonalize the reference time series of F10.7, QBOA, QBOB, and MEI (shown in the left column of Fig. R4), and thus their residuals (F10.7_{res}, QBOA_{res}, QBOB_{res}, MEI_{res}, shown in the right column of Fig. R4) can be

obtained and will be used as predictor variables (or explanation variables) after checking and removing their multicollinearity.

The rationality or goodness of the seasonal fitting result is quantified by R^2 score, which is the variations of the raw data explained by the model and defined as follows:

$$R^2 = 1 - \{\sum_{i=1}^{N} u_{res}^2(t_i) / \sum_{i=1}^{N} [u(t_i) - \bar{u}]^2\},\ \bar{u} = \frac{1}{N}\sum_{i=1}^{N} u(t_i). \quad \text{(R4)}$$

The best fitting results in $R^2 = 1$, which means that the fitting result is the same as the raw data. For example, the seasonal fitting of BU at 25°S and 50 km is shown as red line in Fig. R4(a1). It coincides well with the raw BU series (black line in Fig. R4a1) with $R^2 = 0.967$. This means that Eq. R3 explains 96.7% of the variations of BU at 25°S and 50 km. Moreover, for this case, the fitting result shows that the AO has amplitude of 53.9 ms^{-1} and is in the dominant position. Then the SAO has a smaller amplitude of 13.2 ms^{-1}. While the TAO is the weakest and has amplitude of 3.9 ms^{-1}. The rationality of the fitting results (R^2) at other latitudes and heights will be shown in Sect. 3.1.

Table 1: The correlation coefficients and their p-values of regressors

	QBO_{30}		QBO_{10}		ENSO (MEI indx)	
	CC	p-value	CC	p-value	CC	p-value
F10.7	-0.0283	0.6803	0.0003	0.9965	0.2022	0.0030
QBO_{30}			-0.0025	0.9705	0.0368	0.5921
QBO_{10}					-0.0779	0.2567

Second, we check the multicollinearity among the predictor variables, which are the de-seasonalized F10.7, QBO_{30}, QBO_{10}, and MEI. The multicollinearity often leads to meaningless results if the correlation coefficients (CCs) between two or more predictor variables are significant. Here we calculate the CC and p-value of each pair of predictor variables (Table 1). If the p-value of a pair of predictor variables is less than 0.1 (or 0.05), one can state that the CC differs from zero at a confidence level 90% (or 95%). And thus, the multicollinearity of this pair is significant. In contrast, larger p-values indicate lower confidence level and insignificant multicollinearity. Table 1 shows that, the CCs of most pairs are less than 0.1, and p-values are larger than 0.1. This indicates that the multicollinearities of these pairs are insignificant and are approximately independent. On exception is the pair of F10.7 and ENSO, which has a CC of 0.2022 with p-value of 0.0030. This indicates that the multicollinearity of F10.7 and ENSO is significant at confidence level of 95%. To improve the independency between F10.7 and ENSO, a linear regression is performed with response variable of MEI index and predictor variable of F10.7. The residual of MEI index, which excludes the influences of F10.7, is used as a predictor variable to represent the effects of ENSO in the following

MLR model. We note that the residual of MEI index is still noted as MEI_{res} in the following text. Now, the multicollinearity among the four predictor variables can be neglected and ensures a meaningful result of MLR in the next step.

Third, MLR is applied to get the responses of the de-seasonalized winds (i.e., u_{res} in Eq. R3) to the four predictor variables ($\mathrm{F10.7}_{res}$, QBOA_{res}, QBOB_{res}, MEI_{res}) prepared in the second step. The MLR model is written as:

$$u_{res}(t_i) = \alpha \mathrm{F10.7}_{res}(t_i) + \beta_A \mathrm{QBOA}_{res}(t_i) + \beta_B \mathrm{QBOB}_{res}(t_i) + \gamma \mathrm{MEI}_{res}(t_i) + \eta t_i + \varepsilon(t_i) \quad \text{(R5)}$$

The regression coefficients $\alpha, \beta_A, \beta_B, \gamma$ indicate the responses of wind to F10.7, QBOA, QBOB, and MEI, respectively. The regression coefficient η is the linear variations or long-term trend. $\varepsilon(t_i)$ is the residual of the fitting and can be used to estimate the standard deviation and the p-value of each coefficient with the help of variance-covariance matrix and student-t test (Kutner et al., 2004; Mitchell et al., 2015). The monthly responses are obtained by selecting t_i in Eq. (R5) only in that month of each of year. E.g., the response in January can be obtained by selecting the data only in January of each year. The annual responses are obtained by using all the data during 2002–2019.

3. Multicollinearity: In the MLR analysis, multicollinearity often leads to meaningless results. The authors need to evaluate and indicate whether the correlations between regressors are sufficiently small before performing the MLR analysis.

Response: Following your suggestion, we have evaluated the multicollinearity of each pair of regressors in this version. Please see the second step in Responses#2 and in Sec. 2.2 of the text. We rewrite here to close the responses:

Table 1: The correlation coefficients and their p-values of regressors

	QBO_{30}		QBO_{10}		ENSO (MEI indx)	
	CC	p-value	CC	p-value	CC	p-value
F10.7	-0.0283	0.6803	0.0003	0.9965	0.2022	0.0030
QBO_{30}			-0.0025	0.9705	0.0368	0.5921
QBO_{10}					-0.0779	0.2567

Here we calculate the CC and p-value of each pair of predictor variables (Table 1). If the p-value of a pair of predictor variables is less than 0.1 (or 0.05), one can state that the CC differs from zero at a confidence level 90% (or 95%). And thus, the multicollinearity of this pair is significant. In contrast, larger p-values indicate lower confidence level and insignificant multicollinearity. Table 1 shows that the CCs of most pairs are less than 0.1, and p-values are larger than 0.1. This indicates that the multicollinearities of these predictor variables are insignificant and are approximately independent. On exception is the pair of F10.7 and ENSO, which has a CC of 0.2022 with p-value of 0.0030. This indicates that the multicollinearity of F10.7 and ENSO is significant at confidence

level of 95%. To improve the independency between F10.7 and ENSO, a linear regression is performed with response variable of MEI index and predictor variable of F10.7. The residual of MEI index, which excludes the influences of F10.7, is used as a predictor variable to represent the effects of ENSO in the following MLR model.

4. Statistical significance: In this manuscript, the regression coefficient is considered statistically significant if it is greater than 1σ. However, there is no description of how σ is calculated. In addition, when determining whether a regression coefficient is statistically significant in the MLR analysis, it is common practice to use the p-value of each regression coefficient. Unless there is a special reason to use σ, the p-value should be used (e.g., Mitchell et al. (2015)).

Response: Following your suggestion, we have used the p-value to determine whether a regression coefficient is statistically significant in the new version.

The standard deviation is calculated by the variance-covariance matrix and the residuals of the MLR model (Chapter 6 of Kutner et al. (2004). For a MLR model of,

$$Y_{n\times 1} = X_{n\times p}B_{p\times 1} + \boldsymbol{\epsilon}$$

Here $X_{n\times p}$ is the predictor matrix with p columns (the number of predictor variables) and n rows (observation times or sampling points). $Y_{n\times 1}$ is the response variable with observations times of n. $B_{p\times 1} = \{b_i : i = 0, 1, \cdots, p-1\}$ is the expected regression coefficients of predictor variables. $\boldsymbol{\epsilon}$ is a vector of independent normal random variables. Due to the estimated $B_{p\times 1}$ by MLR model is unbiased, the variance-covariance matrix of $B_{p\times 1}$,

$$s^2\{B\}_{p\times p} = \begin{bmatrix} s^2\{b_0\} & s\{b_0, b_1\} & \cdots & s\{b_0, b_{p-1}\} \\ s\{b_1, b_0\} & s^2\{b_1\} & \cdots & s\{b_1, b_{p-1}\} \\ \vdots & \vdots & & \vdots \\ s\{b_{p-1}, b_0\} & s\{b_{p-1}, b_1\} & \cdots & s^2\{b_{p-1}\} \end{bmatrix} = \frac{\sum_{j=1}^{n}\epsilon_j^2}{n-p}\cdot(X'X)^{-1}$$

The significance of the difference between b_i and 0 can be estimated by student-t test. For the confidence level of 1-α, student-t test states that,

$$\begin{cases} |b_j/s\{b_j\}| \le t(1-\alpha/2\,; n-p), & b_i = 0 \\ |b_j/s\{b_j\}| > t(1-\alpha/2\,; n-p), & b_i \neq 0 \end{cases}.$$

Then the p-value is calculated from t-distribution table with $n-p$ degrees of freedom and α, that describes how likely to find a particular set of observations if the null hypothesis (i.e., the regression coefficient is 0) were true. The smaller the p-value, the more likely to reject the null hypothesis and accept the no-null hypothesis (i.e., the regression coefficient is significant)

5. Impact of SSW: In general, if the effect of SSW is large, it should occur that the regression coefficient is not statistically significant despite its large value. The authors should first check to see

if this is the case, especially in the high latitudes of the winter northern hemisphere.

Furthermore, it is questionable whether it makes sense to apply the MLR analysis to spline interpolated data. Also, it should be explicitly stated which latitude bands were replaced by spline interpolation. Looking at Fig. 10c, it appears that all winters were replaced by spline interpolation, but major SSW does not occur every year. It should be explicitly stated by what criteria SSW is defined.

Response: Following your suggestion and according the $|BU_{Res}|$ shown in Fig. 10 of the new version, we reconstruct the BU at 30°N–50°N and throughout the height range.

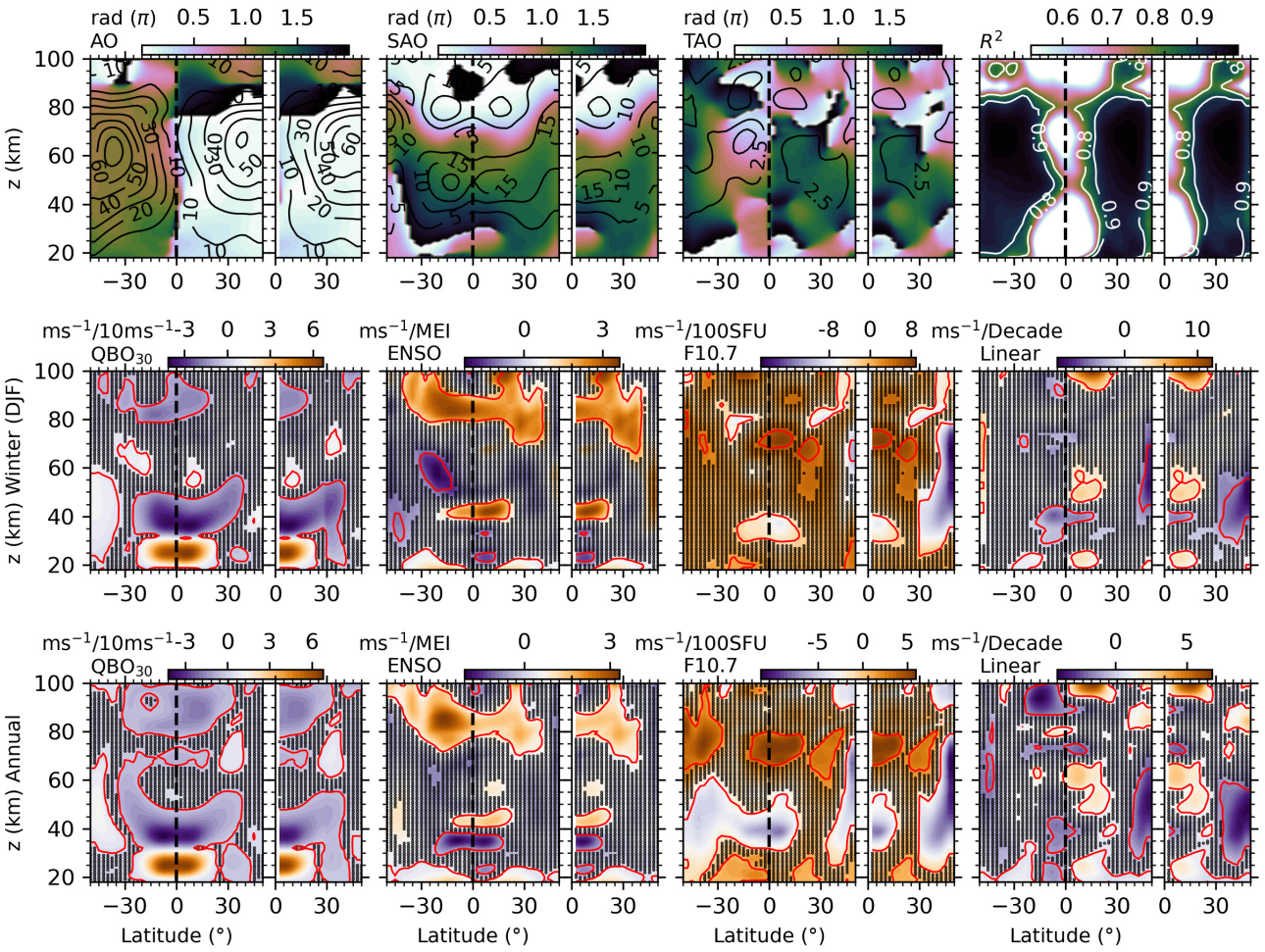

Figure R5: Regression results of the raw (50°S–50°N, left panel of each subplot) and reconstructed BU (0°–50°N, right panel of each subplot) in the NH during 2002–2019. Upper row: seasonal variations. Middle row: the responses of BU to QBO_{30}, QBO_{10}, ENSO, F10.7 and linear variations (from left to right) in winter (December-January-February). Lower row: same caption as the middle row but for those of the annual mean.

According to the major SSW events released by the Chemical Sciences Laboratory of NOAA, (https://csl.noaa.gov/groups/csl8/sswcompendium/majorevents.html), We reconstructed BU only in the winters when the major SSWs occurred (2003, 2004, 2006, 2007, 2008, 2009, 2013, 2018,

2019). Figure R5 shows the amplitudes of seasonal variations and R^2 scores (the first rows), and the responses of reconstructed winds to QBO, ENSO, F10.7, and the linear variations of the raw and reconstructed BU in winter (the second row) and in the annual mean (the third row).

The annual mean responses of the reconstructed and raw BU to QBO_{30} and ENSO are similar on the aspects of both patterns and magnitudes. In contrast, at ~30–60 km and latitudes higher than 30°N, the annual mean responses of the reconstructed BU to F10.7 are more negative and cover a wider region as compared to those of the raw BU. The linear variations of the reconstructed winds are more negative at latitudes higher than 30°N at compared to those of the raw BU.

This has been added in the text.

Minor comments:

6. L. 143-145: Is it safe to consider data from a single point observation as the same as the zonal average, even though it is a monthly average? For example, how does this compare to the data of Smith et al. (2017)?

Response: This point should be clarified. Figure R6 shows the balance winds at the equator reported by Liu et al. (2021) and Smith et al. (2017). It can be seen that the two datasets show a good consistency below ~80 km.

The monthly average of single point observation eliminates the aliasing from migrating tides and traveling planetary waves but contains the non-migrating tides and stationary planetary waves. For the consistency of balance wind and the monthly averaged zonal wind observed at a single station, Figure 3 of Smith et al. (2017) showed that the monthly zonal wind from a meteor radar at Ascension Island (8ºS) coincides well with the balance wind at 81 and 84 km. This indicates that the monthly averaged zonal wind at a single station can represent the zonal average at least below 84 km. While above 84 km, the left column of Figure R6 shows that the theoretical balance winds are mainly eastward (upper panel (a) of the left column). In contrast, the reconstructed winds from a meteor radar observation at Koto Tabang (0.2ºS) are mainly westward. The differences between the theoretical balance wind and meteor radar observations are mainly the tidal aliasing above 84 km (Hitchman and Leovy, 1986; Smith et al., 2017; Xu et al., 2009). Moreover, the comparisons between the reconstructed balance winds with UARP (Atmosphere Research Satellite Reference Atmosphere Project wind climatology) and HWM14 (Horizontal Wind Model, Version 2014) exhibited general consistency above 80 km (Figures 6 and 7 of Liu et al., 2021).

Since the contaminations by non-migrating tides and stationary planetary waves cannot be removed through monthly average at a single station in theory, further validation should be performed by comparing the monthly averaged winds at different longitudes but similar latitudes.

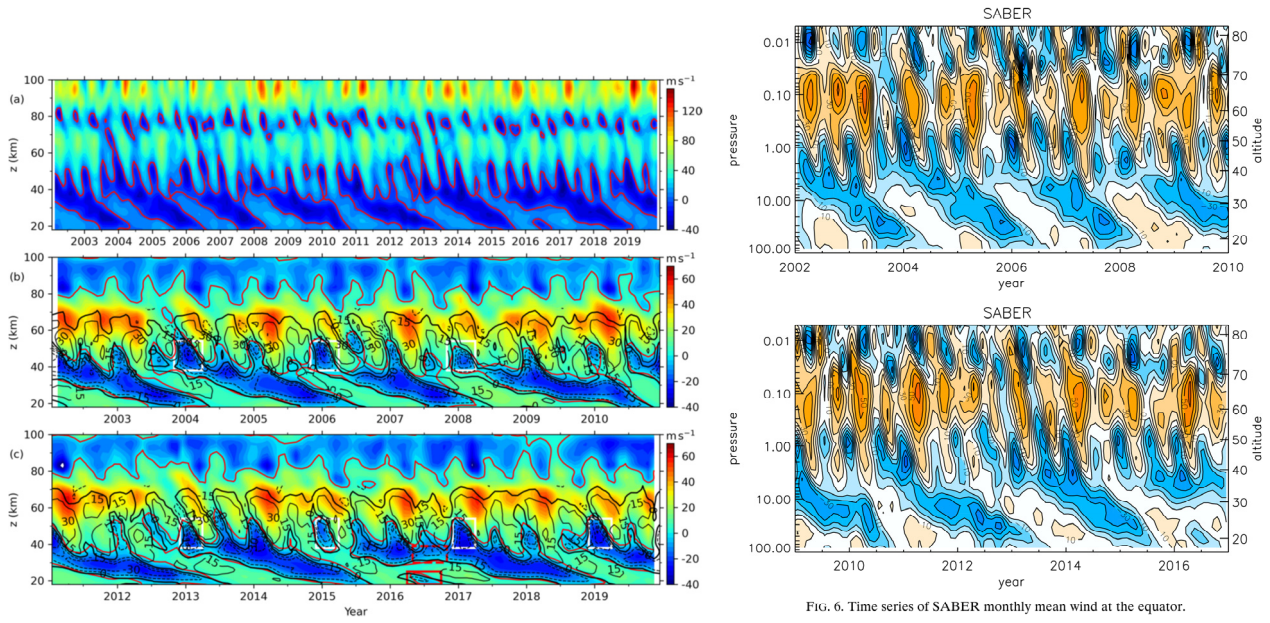

FIG. 6. Time series of SABER monthly mean wind at the equator.

Figure R6: Balance winds at the equator reported by Liu et al. (2021, left column) and Smith et al. (2017, right column). The panel (a) of left column shows the theoretical balance winds from 18 to 100 km. The panels (b) and (c) the reconstructed balance wind, which is the wind in panel (a) replaced by the meteor radar observations at Koto Tabang (0.2ºS) above 80 km.

In the text, we have revised this point as "For the consistency of BU and the monthly averaged zonal wind observed at a single station, Figure 3 of Smith et al. (2017) showed that the monthly zonal wind from a meteor radar at Ascension Island (8ºS) coincides well with the BU at 81 and 84 km. This indicates that the monthly averaged zonal wind at a single station can represent the zonal average at least below 84 km. While above 84 km, Fig. 2(a) of Liu et al. (2021) shows that the theoretical balance winds are mainly eastward. In contrast, the reconstructed winds (Fig. 2b and 2c of Liu et al. (2021)) from a meteor radar observation at Koto Tabang (0.2ºS) are mainly westward. The differences between the theoretical balance wind and meteor radar observations are mainly the tidal aliasing above 84 km (Hitchman and Leovy, 1986; Smith et al., 2017; Xu et al., 2009)"

7. Fig. 2: It is hard to see the phases from the arrows. I recommend to show the amplitudes by contours and the phases by colors.

Response: Following your suggestion, we have revised Fig.2 (Fig. 3 of this version), which shows the amplitudes by contour lines and phases by colors. Please see Fig. R7 below.

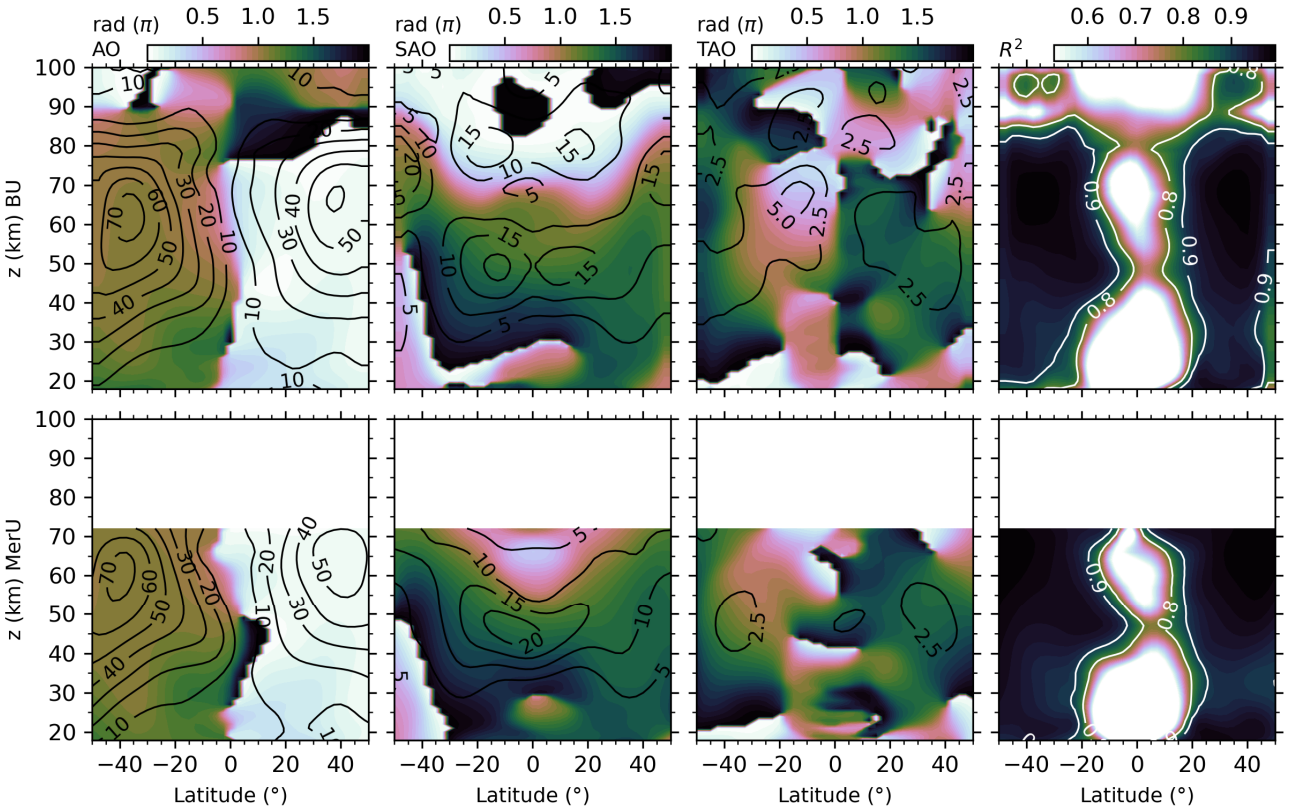

Figure R7: The latitude-height distributions of the amplitudes (contour lines) and phases (color scale) of seasonal variations and the R^2 scores (from left to right) of BU (upper row) and MerU (lower row).

8. L. 237: Please clarify how the annual mean response was calculated. Is it an annual mean of the regression coefficient for each month? Or did you apply the MLR to the data including whole months (216 months)?

Response: In the last version, the regression model is,

$$u(t_i) = A_0 + \text{Season}(t_i) + \alpha \text{F10.7}(t_i) + \beta_{30}\text{QBO}_{30}(t_i) + \beta_{10}\text{QBO}_{10}(t_i) + \gamma \text{ENSO}(t_i) + \eta t_i + \text{Res}(t_i). \quad \text{(R1)}$$

Equation (R1) is applied to data for 18 years. Moreover, the regression coefficients $\alpha, \beta_{30}, \beta_{10}, \gamma, \eta$ are not specific numbers but depend on the month. They have the form of (for example, α):

$$\alpha = \alpha_0 + \sum_{k=1}^{3}[\alpha_{2k-1}\cos(k\omega t_i) + \alpha_{2k}\sin(k\omega t_i)]. \quad \text{(R2)}$$

Here, $\omega = 2\pi/12$ (month). The regression coefficient of F10.7 in January is obtained by setting $t_i = 1$ in Eq. (R2). In a same way, the regression coefficient in February can be obtained by setting $t_i = 2$ in Eq. (R2), and so on. Then we can get the regression coefficients in 12 months. **The annual mean regression coefficient is obtained by averaging the regression coefficients in 12 months.**

In this version, to better explain the MLR model and to remove the collinearity of predictors, the seasonal variations and the responses of wind to F10.7, QBO_{30} (QBOA), QBO_{10} (QBOB), and

MEI are retrieved through steps. Please find details in Responses#2 and in Sec.2.2 of the text. A summary is below:

First, we de-seasonalize the wind and reference time series by fitting the seasonal variations through the least squares method.

Second, we check the multicollinearity among the predictor variables, which are the de-seasonalized F10.7, QBO_{30}, QBO_{10}, and MEI. The multicollinearity of F10.7 and MEI is removed through linear regression with predictor variable of F10.7 and response variable of MEI.

Third, MLR is applied to the de-seasonalized winds (i.e., u_{res} in Eq. R3) to the four predictor variables ($F10.7_{res}$, $QBOA_{res}$, $QBOB_{res}$, MEI_{res}) and is written as:

$$u_{res}(t_i) = \alpha F10.7_{res}(t_i) + \beta_A QBOA_{res}(t_i) + \beta_B QBOB_{res}(t_i) + \gamma MEI_{res}(t_i) + \eta t_i + \varepsilon(t_i) \quad (R4)$$

The monthly responses are obtained by selecting t_i in Eq. (R4) only in that month of each of year. E.g., the response in January can be obtained by selecting the data only in January of each year. The annual responses are obtained by using all the data during 2002–2019.

9. L. 275: higher southern (northern) latitudes in summer (winter) → higher latitudes in the winter hemisphere

Response: Following your suggestion, we have revised as "the responses extending to higher latitudes in winter hemisphere".

10. L. 275-277: I cannot see the signal at 50S/N at z=50-80 km.

Response: Indeed, the signal is weak in this region. The positive responses can be judged through p-values since the regression coefficients around zero have larger p-values, which have been indicated by black dots. In this version, the p-value of 0.1 is indicated by red contour lines. The responses at 50°S circled by the red contour lines, which extend from 30°N to 50°S. Thus, we judge that the responses at 50°S are positive. However, the responses are negative at 50°N.

We have revised in the text as "Moreover, the annual mean responses of BU and MerU to QBO_{30} and QBO_{10} are positive and significant at 50°S at ~z=50–80 km. In contrast, the responses of winds to QBO_{30} and QBO_{10} are negative and have smaller values with p-values less than 0.1".

11. L. 381-420: Trend fitting is sensitive to the values at both edge points. The authors need to mention this point.

Response: You are right. We have added this in the text as "The linear variations of both BU and MerU depend strongly on the temporal intervals and on the values at both edge points".

12. L. 455-456: I think that the seasonal asymmetry is explained by semiannual and terannual

components to some extent.

Response: Thanks for your suggestion. We have added this in the text as "The seasonal asymmetry of zonal winds might be induced by SAO and TAO".

References:

Liu, X., Xu, J., Yue, J., Yu, Y., Batista, P. P., Andrioli, V. F., Liu, Z., Yuan, T., Wang, C., Zou, Z., Li, G., and Russell III, J. M.: Global balanced wind derived from SABER temperature and pressure observations and its validations, Earth System Science Data, 13, 5643–5661, https://doi.org/10.5194/essd-13-5643-2021, 2021.

Mitchell, D.M., Gray, L.J., Fujiwara, M., Hibino, T., Anstey, J.A., Ebisuzaki, W., Harada, Y., Long, C., Misios, S., Stott, P.A. and Tan, D. (2015), Signatures of naturally induced variability in the atmosphere using multiple reanalysis datasets. Q. J. R. Meteorol. Soc., 141: 2011-2031. https://doi.org/10.1002/qj.2492

Smith, A. K., Garcia, R. R., Moss, A. C., and Mitchell, N. J.: The semiannual oscillation of the tropical zonal wind in the middle atmosphere derived from satellite geopotential height retrievals, Journal of the Atmospheric Sciences, 74, 2413–2425, https://doi.org/10.1175/JAS-D-17-0067.1, 2017.

Hitchman, M. H. and Leovy, C. B.: Evolution of the zonal mean state in the equatorial middle atmosphere during October 1978-May 1979, J. Atmos. Sci., 43, 3159–3176, https://doi.org/10.1175/1520-0469(1986)043<3159:EOTZMS>2.0.CO;2, 1986.

Responses to RC2:

General comments:

This paper describes variations in zonal mean zonal wind related to the annual cycle, the semiannual cycle, a terannual cycle, the QBO, ENSO, solar activity, and overall trend during 2002-2019, in the layer 18-100 km and latitude band 50S–50N. The data set analyzed, named "BU", was created from SABER temperatures. Results compare favorably with results from applying the same analysis technique to MERRA2 data. This paper shows that using zonal mean SABER data, supplemented by a single station of Meteor wind station data above 80 km in the tropics, does a good job of characterizing atmospheric variations zonal mean zonal wind variations at time scales longer than a month or so. Several interesting aspects are described, including an unusual response in the summer SH, which will be useful for other investigators to compare and maybe puzzle over. I recommend publication with minor revision, but have a few questions and a few recommendations for helping the reader to grasp the main approach more quickly.

Response: Thanks for your valuable comments and recommendations on our manuscript. Please see the point-to-point responses below.

Questions and recommendations:

1. It took me several pages (line 137) to figure out what part of the atmosphere you were going to investigate. I would recommend including the altitude range in the title and abstract. The title could be something like "Variation in global zonal wind in the layer 18-100 km due to solar activity, the QBO, and ENSO during 2002-2019". I would recommend also adding the latitude range 50°S-50°N to the abstract.

Response: Following your suggestion, the title has been revised as "Variations in global zonal wind from 18 to 100 km due to solar activity, and QBO, ENSO during 2002–2019".

In the abstract, we have added the "from 50°S to 50°N", this sentence is revised as "Due to the difficulty of directly measuring zonal wind from the stratosphere to the lower thermosphere, we derived the global balance wind (BU) from 50°S to 50°N and during 2002–2019 using the gradient wind approximation and SABER temperatures and modified by meteor radar observations at the equator".

2. L33-37: It is hard to understand the mathematical sense of the relationships being described. Please explain more clearly. These include:

"The responses to QBO shift from positive to negative and extend from the equator to higher latitudes with the increasing height. " -What does this mean?

"The responses to ENSO and F10.7 are strongest (positive and negatively, respectively) in the southern stratospheric polar jet region below 70 km and exhibit hemispheric asymmetry."

"While above 70 km, the responses of BU to F10.7 and ENSO are mainly positive."

Perhaps it would be helpful to state, for example, that zonal winds are stronger in location x when y is happening.

"Both BU and MerU exhibit similar linear changes" – increasing? decreasing?

Response: Thanks for your suggestion. We have revised them in the text as "As the increasing of the QBO wind, both BU and MerU change from increasing to decreasing with the increasing height and extend from the equator to higher latitudes. Both BU and MerU increase with the increasing of MEI (an indicator of ENSO) and decrease with increasing F10.7 (an indicator of solar activity) in the southern stratospheric polar jet region below 70 km. The responses of winds to ENSO and F10.7 exhibit hemispheric asymmetry. While above 70 km, BU increases with the increasing of MEI and F10.7. The negative linear changes of BU at 50°N are absent in MerU during October–January".

3. L32, SAO: It might be good to add Delisi and Dunkerton (1985) as a reference regarding the time asymmetry of the SAO. Did they or Garcia et al. show a N/S hemispheric asymmetry?

Delisi, D. P., T. J. Dunkerton, Seasonal variation of the semiannual oscillation, J. Atmos. Sci., 45, 2772– 2787, 1988.

Response: Using the balance wind derived from the temperature observations by Nibums7 Stratospheric and Mesospheric Sounder, Delisi and Dunckerton (1998) showed that the SAO is stronger in the first cycle (December–May) than in the second cycle (June–November). Moreover, the seasonal asymmetry of SAO is related to hemispheric difference in planetary waves in winter.

We have added "This coincides with the balance wind derived from the temperature observations by Nibums7 Stratospheric and Mesospheric Sounder (Delisi and Dunkerton, 1988)…" in Sec.3.1.

Also, in the summary of Sec.3.1, we have revised as "The SAOs around 50 km and 80 km are hemispheric asymmetric and stronger in the SH, which coincides with the HRDI observations (Ray et al., 1998) and the balance winds derived from temperature observations by satellites (Delisi and Dunkerton, 1988; Smith et al., 2017)."

4. Introduction: It would be helpful to the reader if you described straight away what motivated you to do this study. (Why this data set?) Perhaps say that it is unique in that it involves SABER

data and it targets the upper stratosphere to mesosphere. Please include information about what other wind climatologies have been made with SABER data. Perhaps include a statement as to how this study extends or goes beyond what was described in Smith et al. (2017).

Response: Thanks for your suggestion. The description on the dataset in the Introduction has been revised as "The BU covers a latitude range of 50°S–50°N with step of 2.5° and height range 18–100 km with step of 1 km and a temporal range of 2002–2019. The BU coincided generally with re-analysis data, empirical wind models and observations by meteor radars and lidar (Liu et al., 2021) and with the balance wind derived by Smith et al. (2017) above the equator region. Thus, we focus on variations and responses of global zonal winds to various factors since the BU is a reasonable candidate to monthly mean zonal wind".

Moreover, in Sec. 2.1, the following has been added "For the consistency of BU and the monthly averaged zonal wind observed at a single station, Figure 3 of Smith et al. (2017) showed that the monthly zonal wind from meteor radar at Ascension Island (8ºS) coincides well with the BU at 81 and 84 km. This indicates that the monthly averaged zonal wind at a single station can represent the zonal average at least below 84 km. While above 84 km, Fig. 2(a) of Liu et al. (2021) shows that the theoretical balance winds are mainly eastward. In contrast, the reconstructed winds (Fig. 2b and 2c of Liu et al. (2021)) from a meteor radar observation at Koto Tabang (0.2ºS) are mainly westward. The differences between the theoretical balance wind and meteor radar observations are mainly the tidal aliasing above 84 km (Hitchman and Leovy, 1986; Xu et al., 2009b; Smith et al., 2017)".

5. L111-113: It might be helpful to include a sentence describing the nature of the diurnal tide bias that you find. For example, with sampling geometry of the LIMS instrument on Nimbus 7 ascending minus descending data orbit data can be used to estimate the tidal amplitude (e.g., Hitchman and Leovy 1986). Is there something like that in the SABER data?

Response: Sure, diurnal tides can be estimated from SABER data by ascending minus descending orbit data. However, the gradient wind theory (Eq. R1), which is used to retrieve the zonal mean wind, does not include the influence of tides.

$$\frac{\bar{u}^2}{a}\tan\varphi + f\bar{u} = -\frac{1}{a\bar{\rho}}\frac{\partial\bar{p}}{\partial\varphi} \quad \text{(R1)}$$

This sentence has been revised as "To overcome the tidal alias above 80 over the equator (Hitchman and Leovy, 1986; Xu et al., 2009b; Smith et al., 2017), we replaced the BU with the zonal wind observed by a meteor radar at Koto Tabang (0.2°S, 100.3°E)".

Hitchman, M. H. and Leovy, C. B.: Evolution of the zonal mean state in the equatorial middle atmosphere during October 1978-May 1979, J. Atmos. Sci., 43, 3159–3176,

https://doi.org/10.1175/1520-0469(1986)043<3159:EOTZMS>2.0.CO;2, 1986.

6. BU data, section 2.1: What is the approximate vertical resolution? What is the latitudinal resolution of the data set? How do you treat the lower boundary condition on geopotential height at the 18 km level? How do you treat the singularity at the equator? If you interpolate across the equator, do you smooth in y, and if so, how far out in latitude?

Response: (1) the vertical and latitudinal resolution: we have added in the text as "The BU dataset includes the monthly mean zonal wind in the height range of 18–100 km with step of 1 km and at latitudes of 50°S-50°N with step of 2.5° from 2002 to 2019".

(2) lower boundary condition and the singularity at the equator: Equation (R1) is used to calculate the balance wind in the latitude ranges of 10°N–50°N and 10°S–50°S;

Above the equator, due to the singularity of Eq. (R1) at the equator, one need to differentiate Eq. (R1) with φ. As $\varphi \to 0$, we have $\tan\varphi \to \varphi$, $\sin\varphi \to \varphi$. Thus, Eq. (R1) can be simplified as (Fleming et al., 1990),

$$\frac{\bar{u}^2}{a} + 2\Omega\bar{u} = -\frac{1}{a\bar{\rho}}\frac{\partial^2\bar{p}}{\partial\varphi^2}. \quad \text{(R2)}$$

According to Fleming et al. (1990) and Smith et al. (2017), the monthly mean zonal mean wind is mainly in the range of ±75ms^{-1}. Thus, the term $\bar{u}^2/a$ is one to two orders smaller than $2\Omega\bar{u}$ and can be neglected. Then, $\bar{u}$ at the equator can be expressed as (Fleming et al. 1990; Swinbank & Ortland, 2003),

$$\bar{u} = -\frac{1}{2\Omega a\bar{\rho}}\frac{\partial^2\bar{p}}{\partial\varphi^2}. \quad \text{(R3)}$$

It is not necessary to use lower boundary condition in Eq. (R3). It should be noted that, the lower boundary is necessary if the thermal wind equation is expressed as (Eq. 3 of Xu et al., 2009a),

$$\frac{\partial\bar{u}}{\partial z} = -\frac{g}{2\Omega a\bar{T}}\frac{\partial^2\bar{T}}{\partial\varphi^2}. \quad \text{(R3)}$$

(3) Interpolation: At 2.5°N-7.5°N and 2.5°S-7.5°S, the BU is estimated by a cubic spline interpolation of the BU at 10°N-50°N, 10°S-50°S and the reconstructed BU at the equator.

In the text, we have clarified this point in the text as:

Equation (1) is used to calculate the BU in the latitude ranges of 10°N–50°N and 10°S–50°S. Above the equator, the BU is calculated as $\bar{u} = -(\partial^2\bar{p}/\partial\varphi^2)/(2\Omega a\bar{\rho})$. At 2.5°N–7.5°N and 2.5°S–7.5°S, the BU is estimated by a cubic spline interpolation of the BU at 10°N–50°N, 10°S–50°S and the reconstructed BU at the equator. The detailed description can be found in Liu et al. (2021).

Fleming, E. L., Chandra, S., Barnett, J. J., and Corney, M.: Zonal mean temperature, pressure, zonal wind and geopotential height as function of latitude, Adv. Space Res., 10, 11–59,

https://doi.org/10.1016/0273-1177(90)90386-E, 1990.

Swinbank, R. and Ortland, D. A.: Compilation of wind data for the Upper Atmosphere Research Satellite (UARS) Reference Atmosphere Project, J. Geophys. Res., 108, 4615, https://doi.org/10.1029/2002jd003135, 2003.

7. Figure 1 caption and text: You show results which must be for particular locations, but you don't say where they are! Each of the responses varies in latitude and altitude. For Fig. 1g, please state information about altitude, latitude, and the meaning of coefficients within the figure caption, instead of above the plot. For each of the plots in the right-hand column please state the latitude and altitude that you are referring to. In the text it seems important to clarify that these are sample points, not global indices, and that the response varies in space.

Response: Figure 1 is separated into two Figures (Fig. R1 and R2) in the new version. Now, the new Fig.R1 and its caption is revised as:

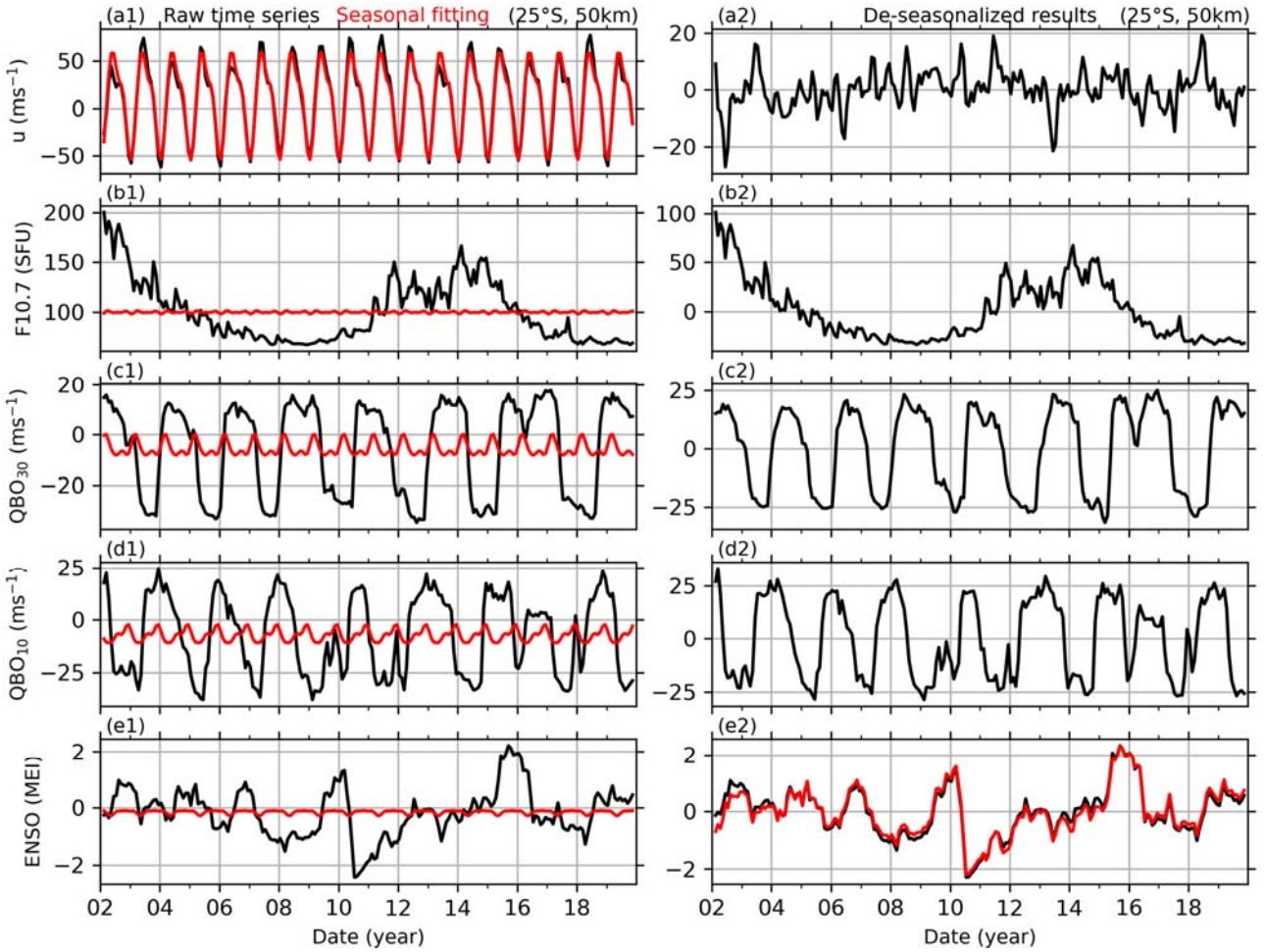

Figure R1: Example of the reference time series (left column) and their de-seasonalized results (right column). The first row: BU at 25°S and 50 km (black line in a1) and its seasonal fitting result (red line in a1), and the residual of BU (black line in a2)). The second, third, and fourth rows: same

captions as the first row but for solar activity (indicated by F10.7), QBO at 30 hPa (QBO_{30} or QBOA) and at 10 hPa (QBO_{10} or QBOB), and ENSO (indicated by MEI index).

At the beginning of Sec.2.2, we have added "The detailed applications of MLR to retrieve the seasonal variations of winds and the responses of winds to F10.7, QBOA, QBOB, and MEI can be ascribed to the following three steps. For illustrative purpose, BU at 25°S and 50 km (black in Fig. 1a1) is taken as an example to show the procedure of MLR. This procedure is also applied to winds at other latitudes and heights, but results in different regressions coefficients due to the latitudinal and height dependencies of the seasonal variations and the responses of winds to F10.7, QBOA, QBOB, and MEI".

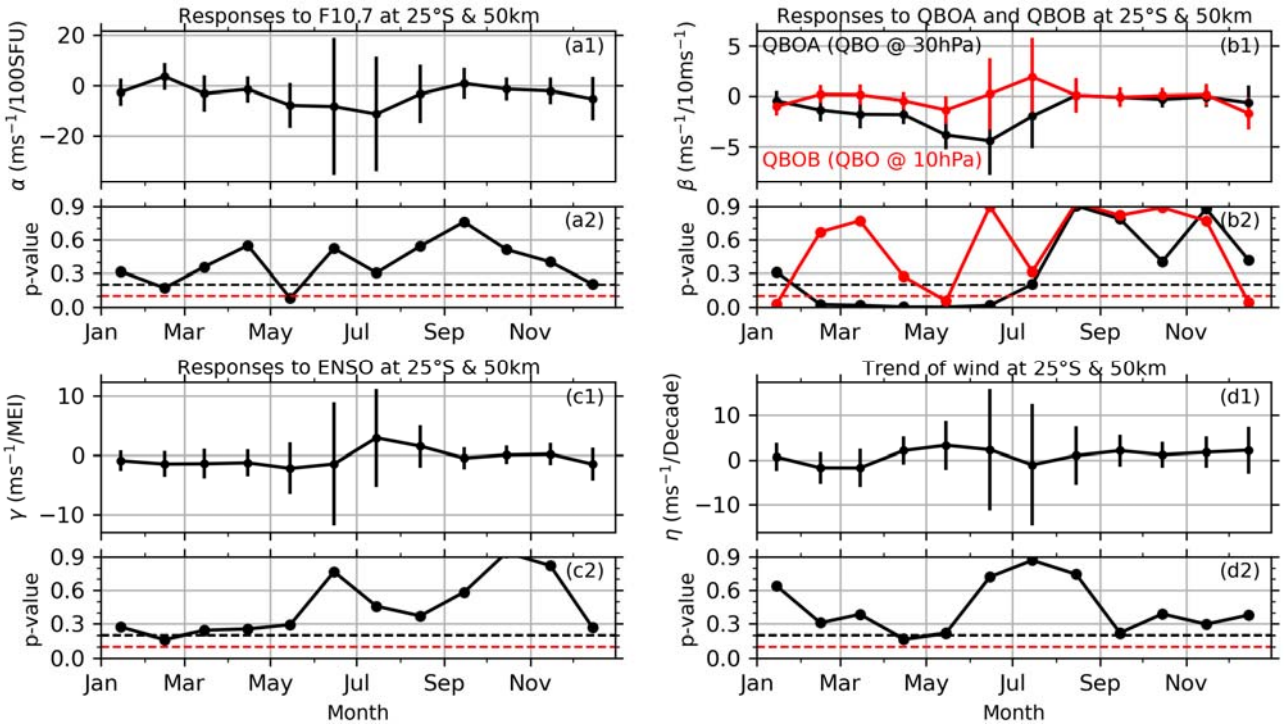

Figure R2: Example of retrieving the monthly responses of BU at 25°S and 50 km (upper subplot of each panel) and their p-values (lower subplot of each panel) to solar activity (a1 and a2) QBOA (black in b1 and b2) and QBOB (red in b1 and b2), ENSO (c1 and c2), and the linear variations (d1 and d2). The error bars are the confidence interval at 90% confidence level.

We have added the latitude and height in each plot and in the figure caption. Corresponding revisions have been made in the last paragraph of Sec.2.2.

8. L187-188: Fig. 1b shows that there is only a strong response during boreal summer.

Response: Following your suggestion, we have added this in the text as "The responses of BU

at 25°S and 50 km to QBO_{30} and QBO_{10} (Fig. 2b1) have annual means of -1.2 ms^{-1}/10 ms^{-1} (p-value=0.0) and -0.3 ms^{-1}/10 ms^{-1} (p-value=0.22). The monthly responses of BU at 25°S and 50 km to QBO_{30} have negative peaks of ~3–5 ms^{-1}/10 ms^{-1} (p-value<0.1) in April-July, when QBO_{30} reaches its eastward or westward peaks. This indicate that the responses of BU at 25°S and 50 km to QBO_{30} are strong in the boreal summer. However, the monthly responses of BU at 25°S and 50 km to QBO_{10} is much weaker than that to QBO_{30}".

9. L188-189: Please say where these numbers pertain to and perhaps characterize how they vary in latitude/altitude.

Response: We have revised as "The responses of BU at 25°S and 50 km to ENSO (Fig. 2c1) have an annual mean of -0.31 ms^{-1}/MEI (p-value=0.56). The monthly responses of BU at 25°S and 50 km to ENSO have negative peak in May and positive peaks in July and August but have large p-values in May–November. The annual mean linear variations (Fig. 1h) is of 0.99 ms^{-1}/Decade (p-value=0.27). The monthly linear variations of BU at 25°S and 50 km reach a peak of 3 ms^{-1}/Decade (p-value<0.2) in May".

10. Fig. 2, right hand panels: How would short vertical structures, such as those associated with the QBO, be perceived by SABER sampling? Can that contribute to the pattern shown, with reduced "explained variance" in the tropics?

Response: In this version, to elucidate the MLR model better and to remove the collinearity of predictors, the seasonal variations and the responses of winds to F10.7, QBOA, QBOB, and MEI are retrieved through steps. Please find details in Sec.2.2 of the text. A summary is below:

First, we de-seasonalize the wind and reference time series by fitting the following harmonics through the least squares method. At each latitude and height, the wind series is fitted as,

$$u(t_i) = u_0 + \sum_{k=1}^{3} A_k \cos[k\omega(t_i - \varphi_k)] + u_{res}(t_i). \quad \text{(R4)}$$

Second, we check the multicollinearity among the predictor variables, which are the de-seasonalized F10.7, QBO_{30} (QBOA), QBO_{10} (QBOB), and MEI. The multicollinearity of F10.7 and MEI is removed through a linear regression with predictor variable of F10.7 and response variable of MEI.

Third, MLR is applied to get the responses of the de-seasonalized winds (i.e., u_{res} in Eq. R4) to the four predictor variables ($F10.7_{res}$, $QBOA_{res}$, $QBOB_{res}$, MEI_{res}) prepared in the second step. The MLR model is written as:

$$u_{res}(t_i) = \alpha F10.7_{res}(t_i) + \beta_A QBOA_{res}(t_i) + \beta_B QBOB_{res}(t_i) + \gamma MEI_{res}(t_i) + \eta t_i + \varepsilon(t_i) \quad \text{(R5)}$$

The monthly responses are obtained by selecting t_i in Eq. (4) only in that month of each of year. E.g., the response in January can be obtained by selecting the data only in January of each year. The

annual responses are obtained by using all the data during 2002–2019.

The first step of this version does not include QBO, ENSO, and F10.7. This induces smaller R^2 scores and the disappearance of the small structure, as compared to the last version. Since the amplitudes of QBO is much larger than the those of seasonal variations (Fig. 1d1 and 1d2), we agree your statement that the short vertical structures in the tropics might be associated with QBO.

In this version, we have added "and (4) the strong QBO signals, which were not included in Eq. (2)" as a reason of smaller R^2 scores in the tropical region.

11. L251: I would expect this to vary in space because the zonal wind anomalies are vertical integrals of meridional gradients in temperature anomalies, which may be caused by solar heating anomalies. If most of the modulation of solar heating is in the ozone layer then one could work out or anticipate the corresponding spatial variation in zonal wind anomaly.

Response: Thanks for your suggestion. I agree your idea that the solar heating may influence the zonal wind through the ozone layer. Both ozone and temperature profiles have been measured by the SABER instrument. This provides an opportunity to study the responses of ozone and temperature, as well as their meridional gradient, to the solar heating. This idea will be tested in our future work. We have added this possible idea in the text as "Another possible mechanism is that the modulation of solar heating in the ozone layer, which influences the meridional gradient of temperature and thus the zonal wind. However, this mechanism should be validated through observations or simulations".

12. Figs. 3 and 5: It seems unusual that during July in the SH there is a strong signal in both F10.7 and ENSO.

Response: You are right. The responses of BU to F10.7 and ENSO are strong during July in the SH. A possible reason is that the waves (gravity waves, non-migrating tides, planetary waves) exhibit stronger variabilities and more complex spatial-temporal structures in the NH than those in the SH. This induces a more complex dynamical coupling between waves and zonal mean wind in the NH than that in the SH. Then the complex dynamical coupling might induce that influences of F10.7 and ENSO to wind are not as obvious in the NH as in the SH. Another possible reason is that the zonal mean wind is stronger in the SH than that in the NH during winter times. Thus, the responses of winds to F10.7 and ENSO are stronger during July in the SH than those in the NH counterpart. Moreover, the responses of winds to QBO_{10} are also stronger in the during July in the SH than those in the NH counterpart.

This has been added at the end of the Sec. 3.4.

13. Fig. 7: The vertical scale of the anomalies associated with the QBO scale like the QBO, but what can account for the pancake structures in the ENSO anomalies in the lower panels?

Response: Thanks for your careful reading. The pancake structures in ENSO anomalies can also be seen in the 40 years MERRA2 data (MerU40, middle row of Fig. R3) but are not as significant as that in the 18 years MERRA2 data (MerU18, lower row of Fig. R3). Moreover the pancake structures can also be seen in the responses of the zonal mean temperature to ENSO (Fig R4). The physics behind should be further explored.

We have added a note in the text as "We note that the pancake structures in the responses of winds to QBO are likely induce by the propagation nature of QBO. Similar pancake structures can also be seen in the responses of wind to ENSO".

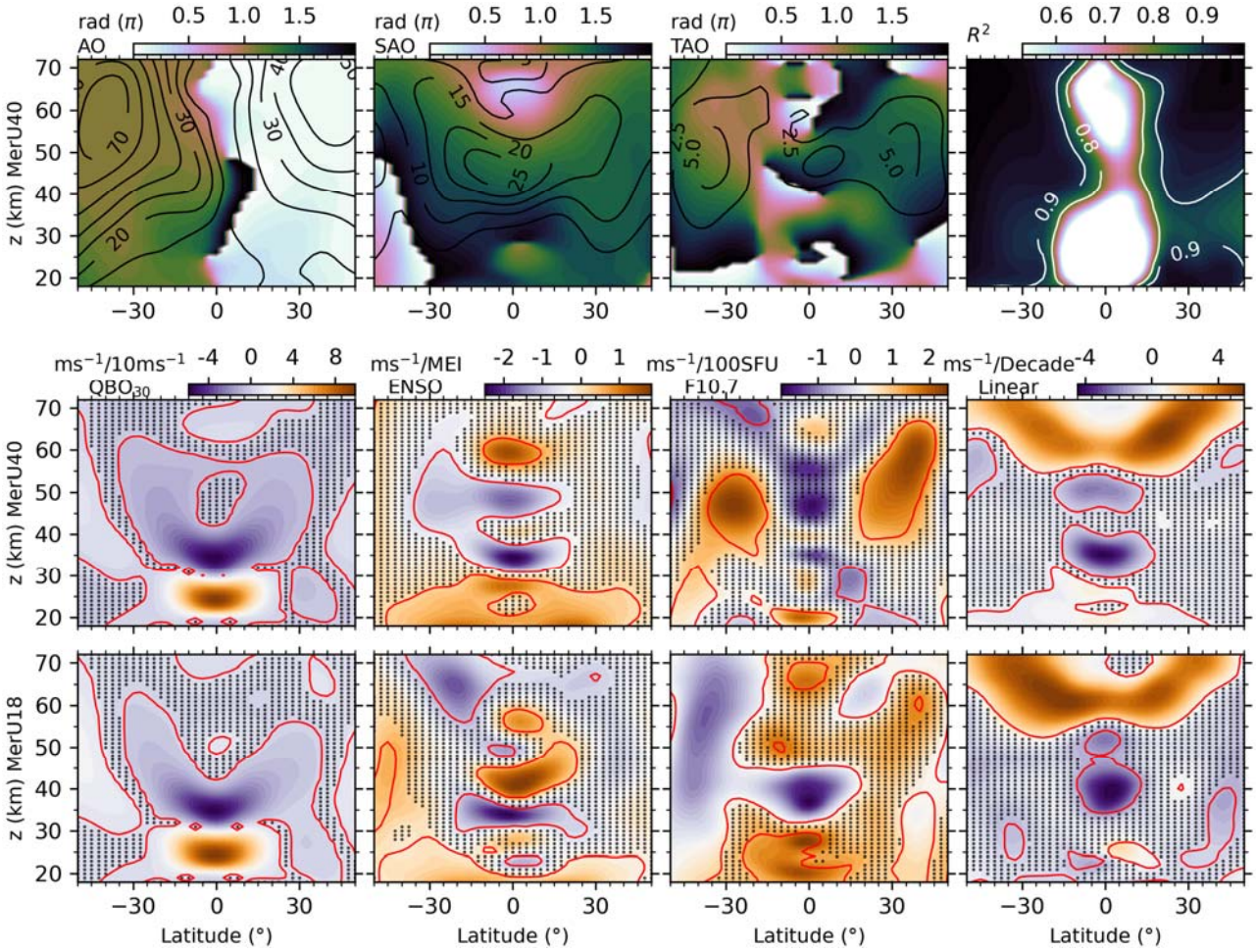

Figure R3: Upper row: the latitude-height distributions of the amplitudes (contour lines) and phases (color scale) of seasonal variations and the R^2 scores (from left to right) of MerU40. Middle row: the latitude-height distributions of the responses of MerU40 to QBOA, ENSO, F10.7 and linear variations (from left to right). Lower row: same caption as the middle row but for the MerU18. The black dots indicate that the regression coefficients with p-values larger than 0.2. The

red lines indicate the regression coefficients with p-values of 0.1.

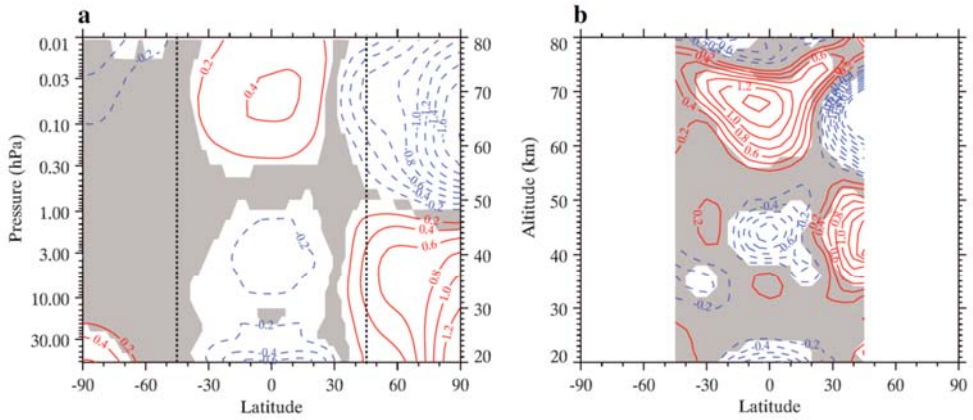

Figure 2. Meridional cross section of zonal mean temperature response to ENSO in winter derived from (a) the WACCM3.5 simulation and (b) the SABER observational data set. The contour interval is 0.2 K/MEI, the blue dash contour lines denote the negative values, and the red solid contour lines denote positive values. The white regions indicate that the results are significant above 95% (1.96σ) confidence level. The vertical black dashed lines denote 45°S and 45°N.

Figure R4: Adopted from Li et al. (2013)

Responses to RC3:

General comments:

The authors derived the global balance wind (BU) in the height range of 18-100 km and latitudes of 50°S–50°N from 2002 to 2019 using the gradient wind approximation and SABER temperatures and modified by meteor radar observations at the equator. Using this data set, the authors examined the responses of zonal wind to QBO, ENSO and solar activity. MERRA2 zonal wind is used to validate BU and its response below 70 km. The manuscript is well organized and easy to follow. The interannual response as a function of month is an interesting result. My main concern is the dataset length and the significance test of the presented coefficients. BU has 18 years of data, to fit interannual response as a function of months, this means there are only 18 data points available for the fit. The manuscript did not present any significance test of fit. Rigorous significance test(s) should be added to make the results trustworthy to readers.

Response: Thanks for your careful reading and suggestions. Following your suggestion, the main improvement of this version can be ascribed to the following three points.

First, to elucidate the MLR model better and to remove the collinearity of predictors, the seasonal variations and the responses of winds to F10.7, QBO30 (QBOA), QBO10 (QBOB), and MEI are retrieved through three steps. Each step has specific purpose and formulae. We note that although the procedures of applying MLR is changed from that in the last version, this does not change the main results and conclusions significantly.

Second, we applied the same MLR procedure to the 40 years (1980–2019) of MERRA2 data (MerU40) and compared with the 18 years (2002–2019) of MERRA2 data (MerU18). Below ~55 km, the consistencies of the responses of MerU18 and MerU40 to QBOA and ENSO are better than those to F10.7 and the linear variations. Moreover, at ~40 km and above the equator, the significant negative linear variations of MerU40 coincide well with those MerU18.

Third, the statistical significance is estimated by p-value, which is used to replace the standard deviation in the last version.

Please see the point-to-point responses below.

More detailed comments:

1. More details should be added to explain the tidal aliasing at the equator. I assume tidal aliasing is not only an issue for 0 degree, it should be the equatorial region. How can a meteor radar station represent the zonal wind in the whole equatorial region? Is there any potential aliasing from semidiurnal tide in the mid latitudes?

Response: You are right, the tidal aliasing is not only an issue for 0 degree but also around the equatorial region. The detailed description on the balance wind (BU) data set can be found in Liu et al. (2021). Here, we provide a short description on the BU and also in the text (Sec. 2.1).

The gradient wind theory is formulated as,

$$\frac{\bar{u}^2}{a}\tan\varphi + f\bar{u} = -\frac{1}{a\bar{\rho}}\frac{\partial\bar{p}}{\partial\varphi} \quad \text{(R1)}$$

Equation (R1) is used to calculate the BU in the latitude ranges of 10°N–50°N and 10°S–50°S.

Above the equator, the BU is calculated as $\bar{u} = -(\partial^2\bar{p}/\partial\varphi^2)/(2\Omega a\bar{\rho})$ (Fleming et al. 1990; Swinbank & Ortland, 2003).

At 2.5°N–7.5°N and 2.5°S–7.5°S, the BU is estimated by a cubic spline interpolation of the BU at 10°N–50°N, 10°S–50°S and the reconstructed BU at the equator. This could remove the aliasing around the equator, at least to some extent.

How can a meteor radar station represent the zonal wind in the whole equatorial region?

Figure R1 shows the balance winds at the equator reported by Liu et al. (2021) and Smith et al. (2017). It can be seen the two datasets show a good consistency below ~80 km.

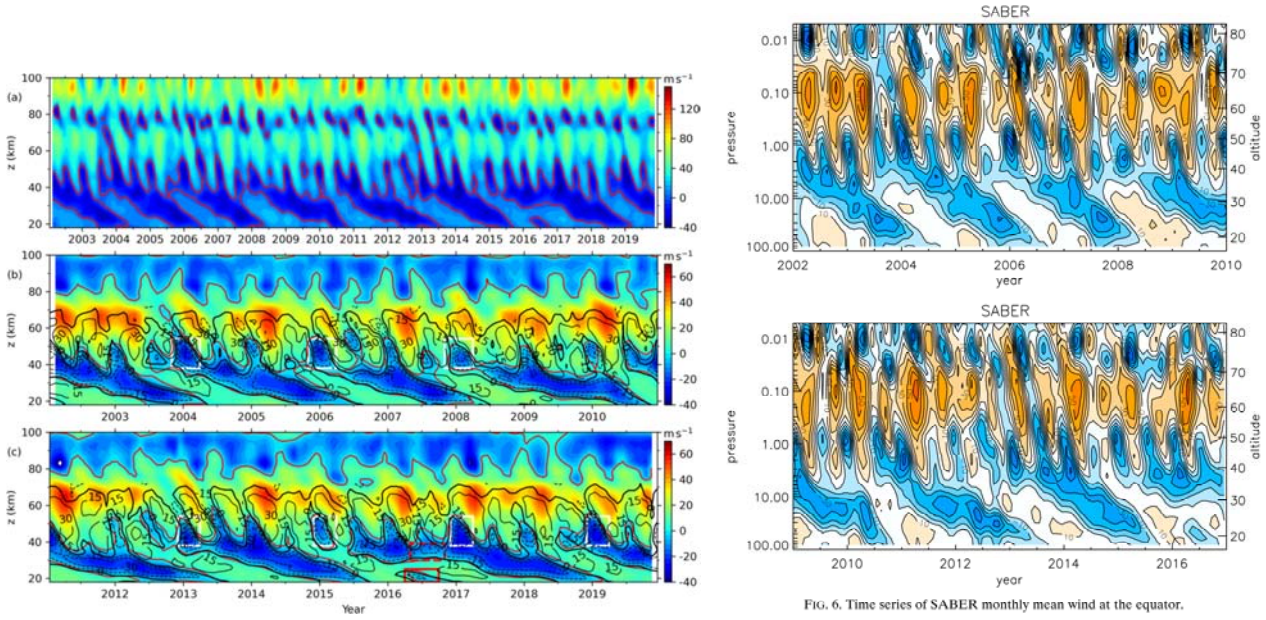

Figure R1: Balance winds at the equator reported by Liu et al. (2021, left column) and Smith et al. (2017, right column). The panel (a) of left column shows the theoretical balance winds from 18 to 100 km. The panels (b) and (c) the reconstructed balance wind, which is the wind in panel (a) replaced by the meteor radar observations at Koto Tabang (0.2ºS) above 80 km.

The monthly average of single point observation eliminates the aliasing from migrating tides and traveling planetary waves but contains the non-migrating tides and stationary planetary waves. For the consistency of balance wind and the monthly averaged zonal wind observed at a single station, Figure 3 of Smith et al. (2017) showed that the monthly zonal wind from a meteor radar at

Ascension Island (8ºS) coincides well with the balance wind at 81 and 84 km. This indicates that the monthly averaged zonal wind at a single station can represent the zonal average at least below 84 km. While above 84 km, the left column of Figure R1 shows that the theoretical balance winds are mainly eastward (upper panel (a) of the left column). In contrast, the reconstructed winds from a meteor radar observation at Koto Tabang (0.2ºS) are mainly westward. The differences between the theoretical balance wind and meteor radar observations are mainly the tidal aliasing above 84 km (Hitchman and Leovy, 1986; Smith et al., 2017; Xu et al., 2009). Moreover, the comparisons between the reconstructed balance winds with UARP (Atmosphere Research Satellite Reference Atmosphere Project wind climatology) and HWM14 (Horizontal Wind Model, Version 2014) exhibited general consistency above 80 km (Figures 6 and 7 of Liu et al., 2021).

Since the contaminations by non-migrating tides and stationary planetary waves cannot be excluded through monthly average at a single station in theory, further validation should be performed by comparing the monthly averaged winds at different longitudes but similar latitudes.

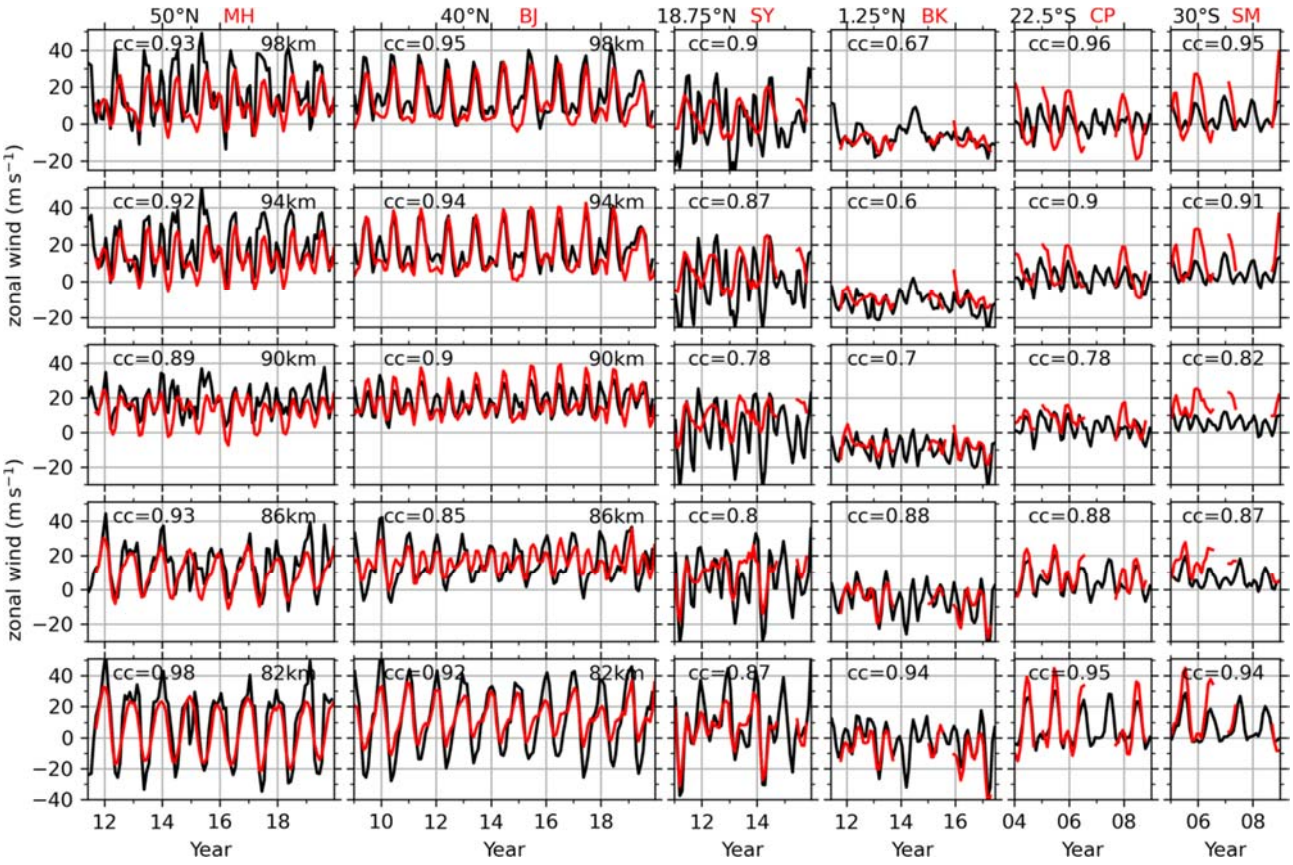

Figure R2: Monthly mean zonal wind from meteor radars (red lines, positive for eastward) at stations (from left to right) of MH (53.5°N), BJ (40.3°N), SY (18.3°N), BK (1.2°S), CP (22.7°S) and SM (29.7°S) and the BU (black) at the similar latitude (labeled on the top of each column) at five heights. The correlation coefficient (cc) between BU and MetU is labeled on each panel. Same y-axis is used in each row. The x-ticks mark the beginning of each year.

Is there any potential aliasing from semidiurnal tide in the mid latitudes?

Liu et al. (2021) compared the BU with meteor radar observations at six stations (Fig. R2). The comparisons among the time series of BU and meteor radar data illustrated that: At MH (53.5°N), BJ (40.3°N), BK (1.2°S) and SM (29.7°S) stations, the agreements between BU and MetU are good in general. The agreements are better at 82 km, 94 km and 98 km than those at 86 km and 90 km. At SY (18.3°N) station, the agreement between BU and MetU is good only at 82 km. At CP (22.7°S) station, the agreement between BU and MetU is good only below 90 km.

We think that the differences between BU and meteor radar data might be induced by the aliasing from semidiurnal tide in the mid latitudes. The first order approximation of momentum equation can be written as,

$$\frac{\bar{u}^2}{a}\tan\varphi + f\bar{u} + \frac{1}{a\bar{\rho}}\frac{\partial\bar{p}}{\partial\varphi} + \underbrace{\left(\frac{1}{a\cos\varphi}\frac{\partial\overline{v'v'}\cos\varphi}{\partial\varphi} + \frac{1}{\rho}\frac{\partial\rho\overline{v'w'}}{\partial z}\right)}_{gravity\ waves,tides,etc.} = 0 \qquad \text{(R2)}$$

When we derive the balance wind, the contribution from waves (gravity waves, tides, etc.) are neglected (the term in the bracket of Eq. R2), which might cause aliasing to the zonal mean wind. Further study should be performed to assess the tidal aliasing on the zonal mean wind.

2. More details should be added to the MLR model especially on how the monthly coefficients for ENSO, QBO, and solar are obtained. How do you deal with the AO, SAO, and TAO when obtaining the monthly coefficients for interannual variability. Line 170, how does 42 parameters come about?

Response: This point should be clarified. In the last version, the regression model is,

$$u(t_i) = A_0 + \mathrm{Season}(t_i) + \alpha\mathrm{F10.7}(t_i) + \beta_{30}\mathrm{QBO}_{30}(t_i) + \beta_{10}\mathrm{QBO}_{10}(t_i) + \gamma\mathrm{ENSO}(t_i) + \eta t_i + \mathrm{Res}(t_i). \qquad \text{(R2)}$$

Equation R2 is applied to data for 18 years. Moreover, the regression coefficients $\alpha, \beta_{30}, \beta_{10}, \gamma, \eta$ are not specific numbers but depend on the month. They have the form of (for example, α):

$$\alpha = \alpha_0 + \sum_{k=1}^{3}[\alpha_{2k-1}\cos(k\omega t_i) + \alpha_{2k}\sin(k\omega t_i)]. \qquad \text{(R3)}$$

Here, $\omega = 2\pi/12$ (month). The regression coefficient of F10.7 in January is obtained by setting $t_i = 1$ in Eq. R3. In a same way, the regression coefficient in February can be obtained by setting $t_i = 2$ in Eq. R3, and so on. Then we can get the regression coefficients in 12 months. The annual mean regression coefficient is obtained by averaging the regression coefficients in 12 months. Moreover, Eq. R2 and (R3) play a role of de-seasonalizing regressor and predictors. This method was proposed by Randel and Cobb (1994) (Eq. 1 and 2 of their paper) and other researchers due to its highly compactable and portable in application.

In this version, to elucidate the MLR model better and to remove the collinearity of predictors, the seasonal variations, and the responses of winds to F10.7, QBO_{30} (QBOA),

QBO_{10} (QBOB), and MEI are retrieved through three steps. Each step has specific purpose and formulae. The detailed revision has been made in the text:

The detailed applications of MLR to retrieve the seasonal variations of winds and the responses of winds to F10.7, QBOA, QBOB, and MEI can be ascribed to the following three steps. For illustrative purpose, BU at 25°S and 50 km (black in Fig. R3a1) is taken as an example to show the procedure of MLR. This procedure is also applied to winds at other latitudes and heights, but results in different regressions coefficients due to the latitudinal and height dependencies of the seasonal variations and the responses of winds to F10.7, QBOA, QBOB, and MEI.

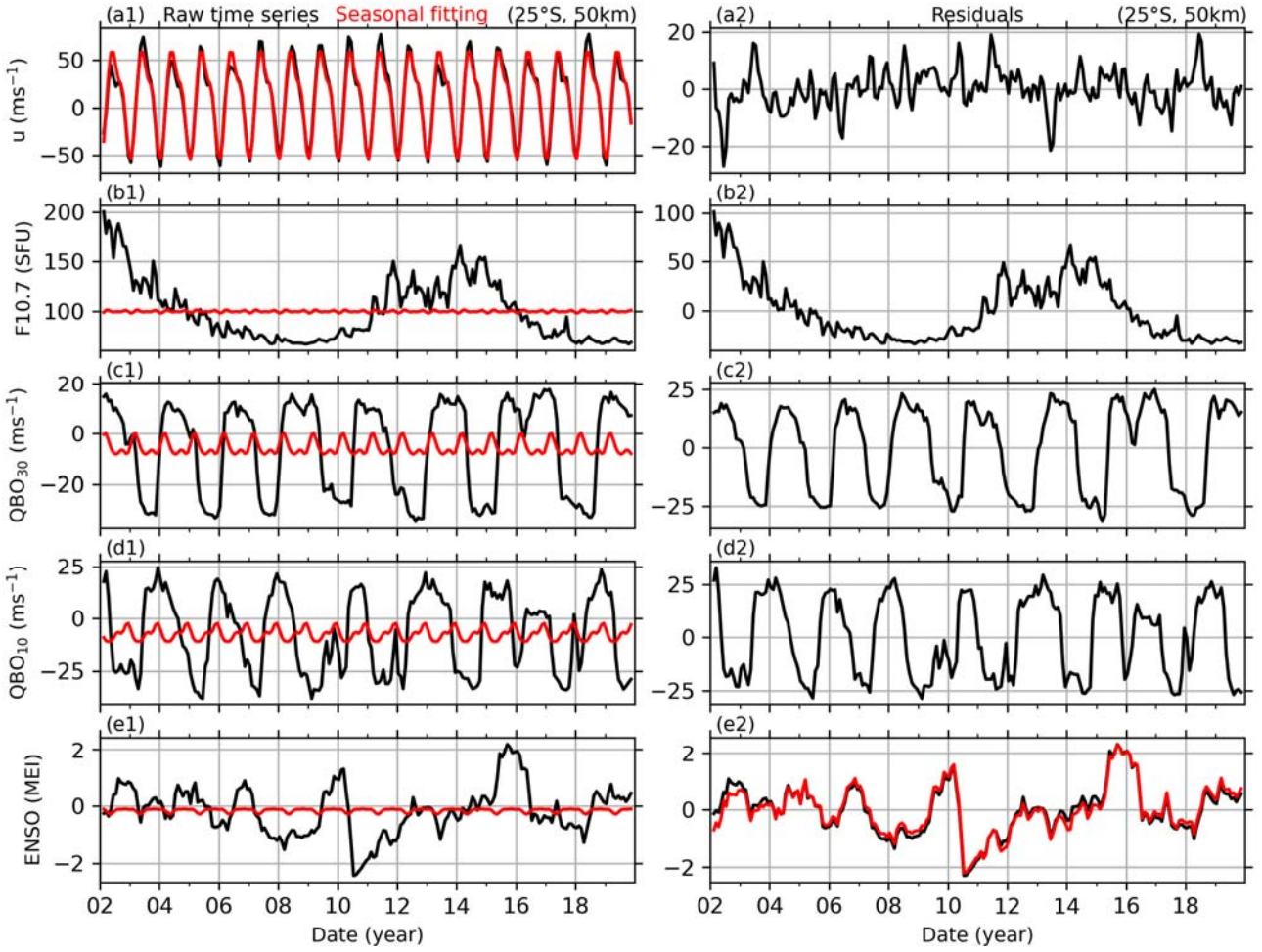

Figure R3: Example of the reference time series (left column) and their de-seasonalized results (right column). The first row: BU at 25°S and 50 km (black line in a1) and its seasonal fitting result (red line in a1), and the residual of BU (black line in a2). The second, third, and fourth rows: same captions as the first row but for solar activity (indicated by F10.7), QBO at 30 hPa (QBO_{30} or QBOA) and at 10 hPa (QBO_{10} or QBOB), and ENSO (indicated by MEI index). The red line in e2 is the residual of MEI index after removing the response of MEI to F10.7.

First, we de-seasonalize the wind and reference time series by fitting the following harmonics through the least squares method. At each latitude and height, the wind series is fitted as,

$$u(t_i) = u_0 + \sum_{k=1}^{3} A_k \cos[k\omega(t_i - \varphi_k)] + u_{res}(t_i). \quad \text{(R4)}$$

Here, t_i $(i = 1, 2 \cdots, N)$ is the month number since February 2002. u_0 is the mean wind over the entire temporal interval, u_{res} is the de-seasonalized wind. $\omega = 2\pi/12$ (month), A_k and φ_k are the amplitude and phase of the annual (AO, $k = 1$), semiannual (SAO, $k = 2$), and terannual (TAO, $k = 3$) oscillations, respectively. In the same way, Eq. R3 is used to de-seasonalize the reference time series of F10.7, QBOA, QBOB, and MEI (shown in the left column of Fig. R3), and thus their residuals (F10.7_{res}, QBOA_{res}, QBOB_{res}, MEI_{res}, shown in the right column of Fig. R3) can be obtained and will be used as predictor variables (or explanation variables).

The rationality or goodness of the seasonal fitting result is quantified by R^2 score, which is the variations of the raw data explained by the model and defined as follows:

$$R^2 = 1 - \{\sum_{i=1}^{N} u_{res}^2(t_i) / \sum_{i=1}^{N} [u(t_i) - \bar{u}]^2\}, \ \bar{u} = \frac{1}{N}\sum_{i=1}^{N} u(t_i). \quad \text{(R5)}$$

The best fitting results in $R^2 = 1$, which means that the fitting result is the same as the raw data. For example, the seasonal fitting of BU at 25°S and 50 km is shown as red line in Fig. R3(a1). It coincides well with the raw BU series (black line in Fig. R3a1) with $R^2 = 0.967$. This means that Eq. R5 explains 96.7% of the variations of BU at 25°S and 50 km. Moreover, for this case, the fitting result shows that the AO has amplitude of 53.9 ms^{-1} and is in the dominant position. Then the SAO has a smaller amplitude of 13.2 ms^{-1}. While the TAO is the weakest and has amplitude of 3.9 ms^{-1}. The rationality of the fitting results (R^2) at other latitudes and heights will be shown in Sect. 3.1.

Table 1: The correlation coefficients and their p-values of regressors

	QBO_{30}		QBO_{10}		ENSO (MEI indx)	
	CC	p-value	CC	p-value	CC	p-value
F10.7	-0.0283	0.6803	0.0003	0.9965	0.2022	0.0030
QBO_{30}			-0.0025	0.9705	0.0368	0.5921
QBO_{10}					-0.0779	0.2567

Second, we check the multicollinearity among the predictor variables, which are the de-seasonalized F10.7, QBO_{30}, QBO_{10}, and MEI. The multicollinearity often leads to meaningless results if the correlation coefficients (CCs) between two or more predictor variables are significant. Here we calculate the CC and p-value of each pair of predictor variables (Table 1). If the p-value of a pair of predictor variables is less than 0.1 (or 0.05), one can state that the CC differs from zero at a confidence level 90% (or 95%). And thus, the multicollinearity of this pair is significant. In contrast, larger p-values indicate lower confidence level and insignificant multicollinearity. Table 1 shows that the CCs of most pairs are less than 0.1, and p-values are larger than 0.1. This indicates that the

multicollinearities of these pairs are insignificant and are approximately independent. On exception is the pair of F10.7 and ENSO, which has a CC of 0.2022 with p-value of 0.0030. This indicates that the multicollinearity of F10.7 and ENSO is significant at confidence level of 95%. To improve the independency between F10.7 and ENSO, a linear regression is performed with response variable of MEI index and predictor variable of F10.7. The residual of MEI index, which excludes the influences of F10.7, is used as a predictor variable to represent the effects of ENSO in the following MLR model. We note that the residual of MEI index is still noted as MEI_{res} in the following text. Now, the multicollinearity among the four predictor variables can be neglected and ensures a meaningful result of MLR in the next step.

Third, MLR is applied to get the responses of the de-seasonalized winds (i.e., u_{res} in Eq. R4) to the four predictor variables ($\mathrm{F10.7}_{res}$, QBOA_{res}, QBOB_{res}, MEI_{res}) prepared in the second step. The MLR model is written as:

$$u_{res}(t_i) = \alpha \mathrm{F10.7}_{res}(t_i) + \beta_A \mathrm{QBOA}_{res}(t_i) + \beta_B \mathrm{QBOB}_{res}(t_i) + \gamma \mathrm{MEI}_{res}(t_i) + \eta t_i + \varepsilon(t_i) \quad \text{(R6)}$$

The regression coefficients $\alpha, \beta_\mathrm{A}, \beta_\mathrm{B}, \gamma$ indicate the responses of wind to F10.7, QBOA, QBOB, and MEI, respectively. The regression coefficient η is the linear variations or long-term trend. $\varepsilon(t_i)$ is the residual of the fitting and can be used to estimate the standard deviation and the p-value of each coefficient with the help of variance-covariance matrix and student-t test (Kutner et al., 2004; Mitchell et al., 2015). The monthly responses are obtained by selecting t_i in Eq. R6 only in that month of each of year. E.g., the response in January can be obtained by selecting the data only in January of each year. The annual responses are obtained by using all the data during 2002–2019.

3. Rigorous significance test should be added. I would suggest a Monte Carlo method. Other methods involve equations have underlying assumptions. If possible, multiple significance test methods should be used. 18 years data is short to study solar cycle, and 18 January is short to get interannual variability on the time scales of 2-5 years (ENSO and QBO) response on a monthly basis.

Response: Thanks for your suggestion, we have used the p-value to determine whether a regression coefficient is statistical significant in the new version.

The standard deviation is calculated by the variance-covariance matrix and the residuals of the MLR model (Chapter 6 of Kutner et al. (2004). For a MLR model of,

$$Y_{n\times 1} = X_{n\times p} B_{p\times 1} + \boldsymbol{\epsilon} \quad \text{(R7)}$$

Here $X_{n\times p}$ is the predictor matrix with p columns (the number of predictor variables) and n rows (observation times or sampling points). $Y_{n\times 1}$ is the response variable with observations times of n. $B_{p\times 1} = \{b_i : i = 0, 1, \cdots, p-1\}$ is the expected regression coefficients of predictor variables. $\boldsymbol{\epsilon}$ is a

vector of independent normal random variables. Due to the estimated $B_{p\times1}$ by MLR model is unbiased, the variance-covariance matrix of $B_{p\times1}$,

$$s^2\{B\}_{p\times p} = \begin{bmatrix} s^2\{b_0\} & s\{b_0,b_1\} & \cdots & s\{b_0,b_{p-1}\} \\ s\{b_1,b_0\} & s^2\{b_1\} & \cdots & s\{b_1,b_{p-1}\} \\ \vdots & \vdots & & \vdots \\ s\{b_{p-1},b_0\} & s\{b_{p-1},b_1\} & \cdots & s^2\{b_{p-1}\} \end{bmatrix} = \frac{\sum_{j=1}^{n}\epsilon_j^2}{n-p}\cdot(X'X)^{-1} \quad \text{(R8)}$$

The significance of the difference between b_i and 0 can be estimated by student-t test. For the confidence level of 1-α, student-t test states that,

$$\begin{cases} |b_j/s\{b_j\}| \le t(1-\alpha/2\,;n-p), & b_i = 0 \\ |b_j/s\{b_j\}| > t(1-\alpha/2\,;n-p), & b_i \ne 0 \end{cases}. \quad \text{(R9)}$$

Then the p-value is calculated from t-distribution table with $n-p$ degrees of freedom and α, that describes how likely to find a particular set of observations if the null hypothesis (i.e., the regression coefficient is 0) were true. The smaller the p-value, the more likely reject the null hypothesis and accept the no-null hypothesis (i.e., the regression coefficient is significant)

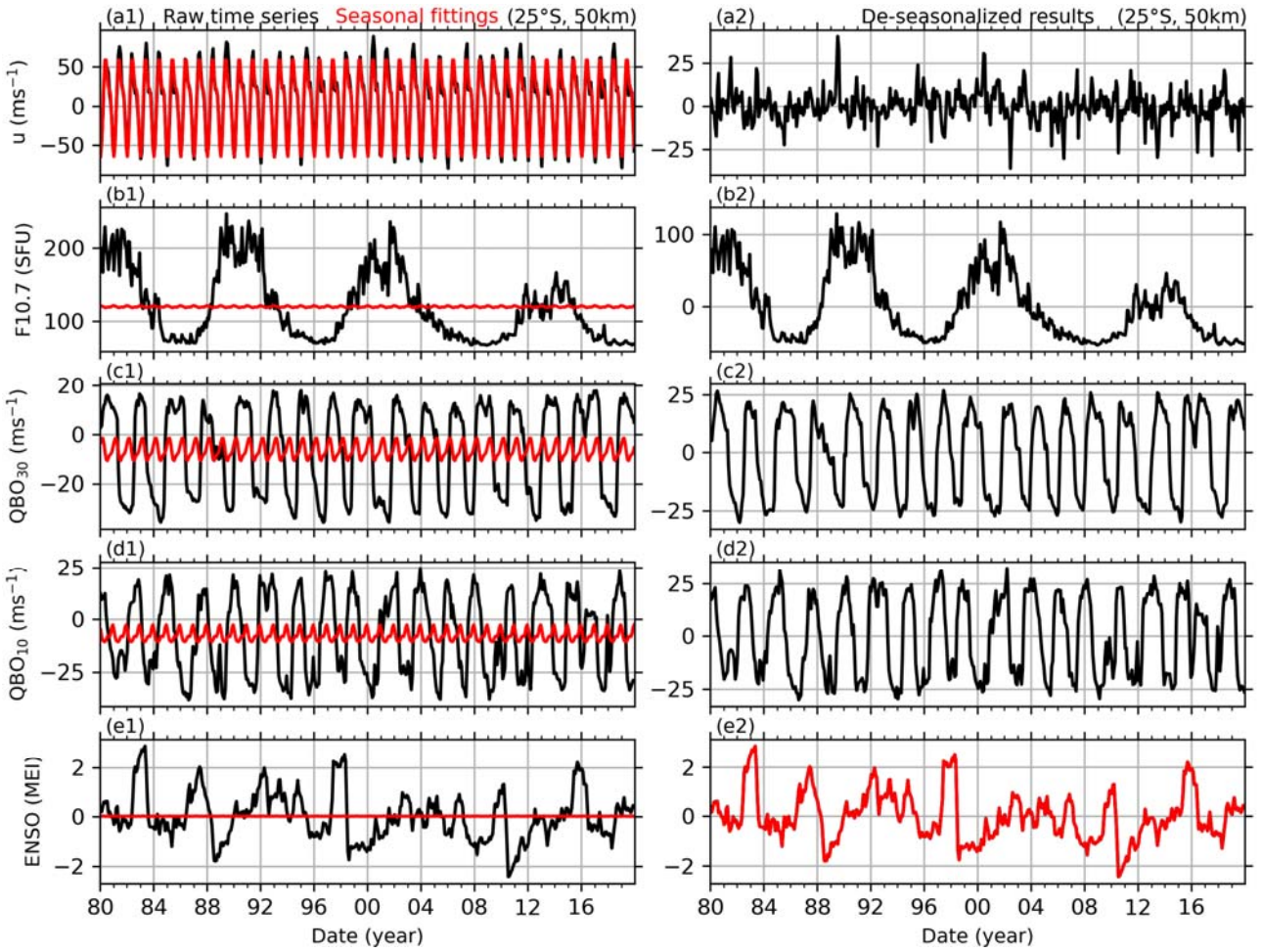

Figure R4: Example of de-seasonalizing MerU40 and the reference time series. The first row: BU at 25°S and 50 km (black line in a1) and its seasonal fitting result (red line in a1), and the residual of BU (black line in a2). The second, third, and fourth rows: same captions as the first row but for

solar activity (indicated by F10.7), QBO 30 hPa (QBO_{30} or QBOA) and 10 hPa (QBO_{10} or QBOB), and ENSO (indicated by MEI index). The red line in e2 is the residual of MEI index after removing the response of MEI to F10.7.

18 years data is short to study solar cycle, and 18 January months is short to get interannual variability on the time scales of 2-5 years (ENSO and QBO) response on a monthly basis.

To clarify this point, we performed the same procedure (see details in Respons#2 and in the text) on the 40 years (1980–2019) of MERRA2 data (MerU40). The monthly zonal mean wind at 25°S and 50 km is taken as an example to show the de-seasonalized results (Fig. R4) and MLR results (Fig. R5).

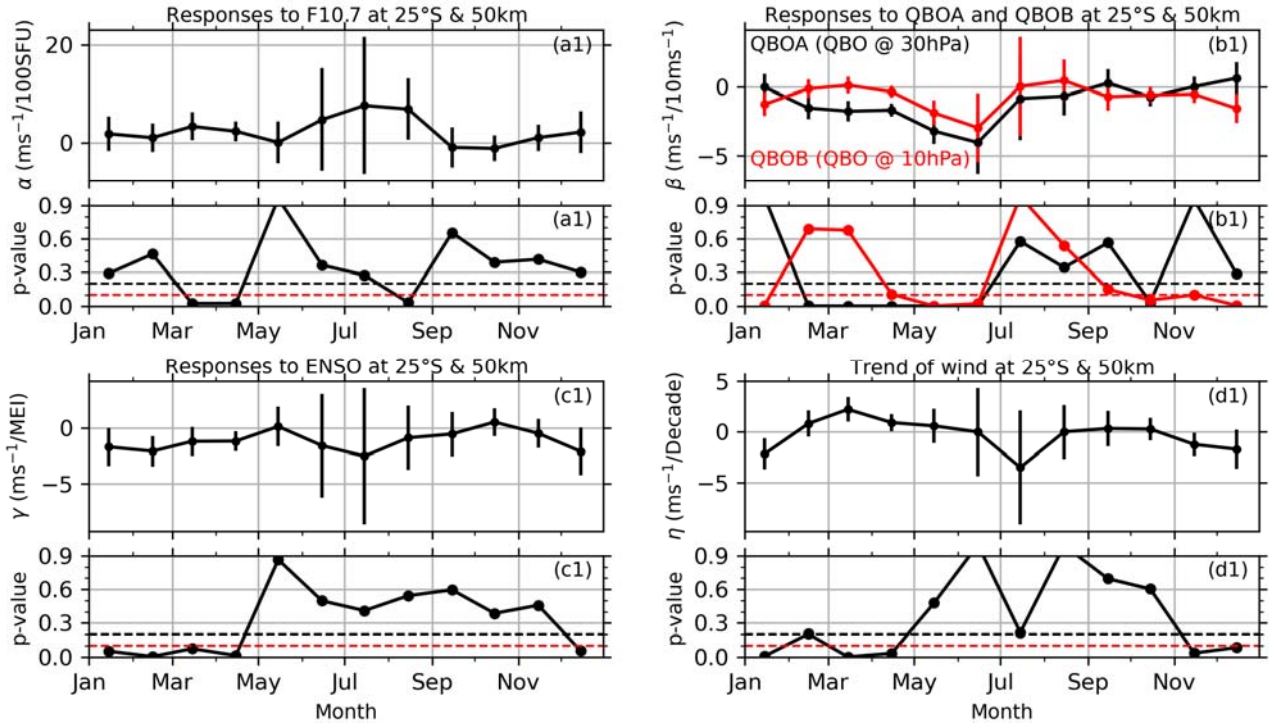

Figure R5: Example of retrieving the monthly responses of MerU40 at 25°S and 50 km (upper subplot of each panel) and their p-values (lower subplot of each panel) to solar activity (a1 and a2) QBOA (black in b1 and b2) and QBOB (red in b1 and b2), ENSO (c1 and c2), and the linear variations (d1 and d2). The error bars are the confidence interval at 90% confidence level.

Figure R4 shows that the seasonal variations are important in the wind (Fig. R4a1 and a2) but are insignificant in the time series of F10.7, QBO_{30} (QBOA) , QBO_{10} (QBOB), and ENSO (Fig. R4b1-e2). Figure R5a1 shows that the responses of MerU40 to F10.7 are significant (p-value ≤ 0.1) in March, April, and August. This is different from the responses of the 18-year data (short for MerU18) to F10.7, which are significant only in May. The responses of MerU40 to QBOA and

QBOB (Fig. R5b1) are significant in April–June and in October. This is similar to those of MerU18, which are also significant in May–June, but insignificant in April and October. The responses of MerU40 to ENSO (Fig. R5c1) are negative and significant in January–April and December. However, the responses of MerU18 to ENSO are also negative but are insignificant. The linear variations of MerU40 (Fig. R5d1) are significant in March and April (positive values) and in November and December (negative values). However, the responses of MerU18 are insignificant (judged by p-value > 0.1) in all months.

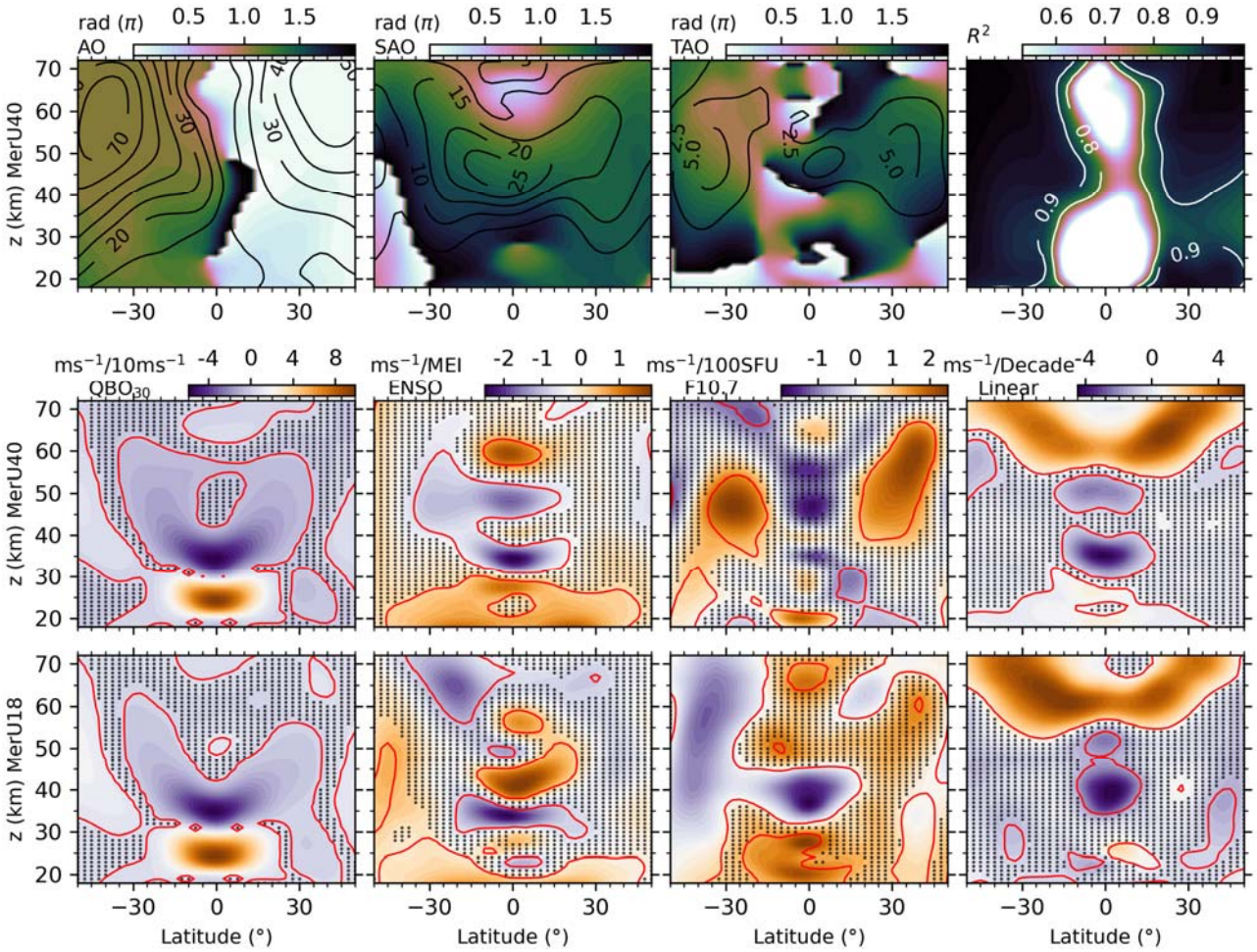

Figure R6: Upper row: the latitude-height distributions of the amplitudes (contour lines) and phases (color scale) of seasonal variations and the R^2 scores (from left to right) of MerU40. Middle row: the latitude-height distributions of the responses of MerU40 to QBOA, ENSO, F10.7 and linear variations (from left to right). Lower row: same caption as the middle row but for the MerU18. The black dots indicate that the regression coefficients with p-values larger than 0.2. The red lines indicate the regression coefficients with p-values of 0.1.

Figure R6 shows the seasonal variations of MerU40 (upper row) and the responses of MerU40 (middle row) and MerU18 (lower row) to various predictors. We see that AO, SAO, and TAO of MerU40 exhibit similar latitude-height distributions as those of the MerU18. The responses of

MerU40 to QBOA are similar to those of MerU18 on the aspects of magnitudes and patterns but have a wider significant region around the equator. Around the equatorial region, the responses of MerU40 to ENSO have similar patterns to those of MerU18 around the equatorial region. However, the positive responses of MerU40 to ENSO are stronger (weaker) than those of MerU18 below ~30 km (around ~40–45 km). Around ~20°S and above ~55 km, the negative responses of MerU18 to ENSO are stronger than those of MerU40. At ~40°S and around ~30 km, the significant positive responses of MerU18 to ENSO cannot be seen in those of MerU40. The significant responses of MerU18 to F10.7 occur in wider height ranges as compared to those of MerU40 around the equator. Moreover, at latitudes higher than 30°S, the responses of MerU18 to F10.7 are negative as compared to the positive responses of MerU40 to F10.7. At around 40°N and ~40–60 km, the positive responses of MerU18 to F10.7 are weaker and less significant than those of MerU40. The linear variations of MerU18 coincide with those of MerU40 above ~30 km, except around ~45°N/S, where the negative linear variations of MerU40 (MerU18) are significant (insignificant). Below ~30 km, the positive linear variations of MerU40 extend to wider latitudes as compared to those of MerU18.

A summary of the responses and linear variations of MerU18 and MerU40 below ~55 km (this is most reliable height since the damping is significant above this height (Ern et al., 2021)) is below. **The consistencies of the responses of MerU18 and MerU40 to QBOA and ENSO are better than those to F10.7 and the linear variations. Moreover, at ~40 km and around the equator, the significant negative linear variations of MerU40 coincide well with those MerU18.**

4. Figure 1 g, the R^2 value is 0.98. This number is somewhat misleading since I assume the goodness of fit is mainly coming from seasonal fit. How good is the fit if only interannual variability is considered?

Response: Comparing the $R^2 = 0.967$ of this version and the $R^2 = 0.98$ of the last version, we see that the goodness of fit is mainly coming from seasonal fit. This confirmed you assumption. This also illustrate that the monthly zonal mean wind (at least for the wind at 25°S and 50 km), the seasonal variations are in the dominant position as compared to the contributions from predictors (F10.7, QBOA, QBOB, ENSO, and linear variations).

The goodness of the fit if only interannual variability is considered can be assessed through ε in Eq. R6 and then the student-t in Eq. R9. If the fitting result is good, this will induce small ε and small variance $s^2\{b_j\}$ in Eq. R8, and then the ratio $|b_j/s\{b_j\}|$ in Eq. R9 should be large. This will provide large probability of accepting $b_i \neq 0$ and high confidence level (small p-value) of estimating b_i. Thus, the p-values shown in Fig. R5 in Responses#3 and Fig. 2 in the text provide an assessment of the goodness of fitting. However, the p-values in Fig. R5 and Fig. 2 are less than 0.1

(confidence level of 90%) only in some limited months. This indicate that the goodness of fitting the interannual variabilities are not as good as that the seasonal fitting results.

Moreover, Fig. 3–7 in the text show that the regions with p-values ≤ 0.1 (confidence level of 90%) occurs only in a limited latitude and height ranges. Thus, the goodness of fitting the interannual variabilities are not as good as that the seasonal fitting results in most latitudes and heights. This might be caused by the dynamic process such as wave-mean flow interaction and the non-uniform distribution of wave sources in the atmosphere, and by the chemical process such as ozone heating in the stratosphere and CO_2 cooling in the mesosphere.

It should be noted that the regions with p-values ≤ 0.1 indicate the responses of the monthly zonal mean wind to predictors are significant.

5. In the discussion of the effects of the data interval, I share another reviewer's point of view: all the data intervals are overlapped somewhat. At least two totally separate data intervals should be used. Significance tests should be added here as well.

Response: I agree with your idea that at least two totally separate data intervals should be used. However, if we separate the 18 years (2002–2019) (MerU18) into two totally separate data intervals, each interval is approximately 9 years, which cannot cover one solar cycle.

To clarify this point, we performed the same procedure on the 40 years (1980–2019) of MERRA2 data (MerU40) (See Responses#3 for detail). Comparing between the results from MerU40 and MerU18, we see that below ~55 km (this is most reliable height since the damping is significant above this height (Ern et al., 2021)), the consistencies of the responses of MerU18 and MerU40 to QBOA and ENSO are better than those to F10.7 and the linear variations. Moreover, at ~40 km and around the equator, the significant negative linear variations of MerU40 coincide well with those MerU18.

Significant tests have been performed through student-t test and p-value.

Responses to Paul Pukite:

Community response to Global zonal wind variations and responses to solar activity, and QBO, ENSO during 2002–2019 (Xiao Liu, Jiyao Xu, Jia Yue, and Vania F. Andrioli)

Attached is an alternate explanation for the periodicity of stratospheric winds. My observation, independent of the acceptability of the paper under review, is that more progress can be made only after refuting the most plausible explanations.

I recommend a fundamental shift of how the mechanisms behind the shifts of stratospheric winds is understood. Much of what I will briefly describe is published in Mathematical Geoenergy (Wiley/AGU, 2018).

Response: Thanks for your recommendation on the point of the mechanisms behind shifts of stratospheric winds. Especially the SAO in the upper stratosphere and QBO in the lower stratosphere. We are very interested in your new insight on the points of QBO, SAO, ENSO., etc. Following your suggestion, we have tried to get the main idea and method of reproducing these oscillations from related references. Such as: (1) the published book (Pukite et al., 2019), (2) some comments on the web: https://geoenergymath.com/tag/qbo/, (3) the model of QBO and ENSO on github: https://github.com/pukpr/GeoEnergyMath/, (4) interactive discussions on the forum: https://forum.azimuthproject.org/discussion/comment/22250/#Comment_22250, (4) many rounds of communications through email.

Pukite, P., Coyne, D., & Challou, D. (2019). Mathematical Geoenergy: Discovery, Depletion, and Renewal (Vol. 241). John Wiley & Sons.

Now, we can reproduce the SAO and QBO according to your idea and detailed explanations through email. See below for the detailed procedure of reproducing QBO wind. It should be noted that there is still room to improve the reproduced QBO wind by us as compared the optimal QBO wind reproduced by you.

First, we assume that the semi-annual cycle in the upper stratosphere is a result of the nodal cycle about the Earth's ecliptic axis. This results in a semi-annual cycle and not annual cycle due to the symmetry of the hemispheres. In terms of a heuristic mathematical construct, this can be formulated by the multiplication of **an annual sinusoidal cycle** convoluted with **a semi-annual delta function impulse train phased according to the (+/-) pairs of solstice or equinox events** – a positive (+) for one seasonal event and negative (-) for the complementary event. From this, a rudimentary square wave time-series is generated, with a semi-annual period resulting from the positive excursions pairing to create a positive and similar for the multiplication of the negative excursions. This is adequate to empirically describe the SAO of the upper stratosphere and identify

it with a forcing and not a resonant condition.

Next, consider that at lower stratospheric altitudes, the QBO cycle of ~28 months takes over. The idea is that a similar nodal construct can be applied but instead of applying only an annual nodal cycling to the convolution, we also add in the nodal lunar tidal cycle. Now we note the important realization that the 0-wavenumber symmetry of the QBO behavior demands that the draconic or nodal lunar cycle of 27.2122 days must be applied to model a global effect (not the longitudinally dependent 27.3216 days cycle associated with regional tides). This is adequate to empirically describe the QBO of the lower stratosphere and identify it with a tidal forcing where the density is greater and thus more susceptible to gravitational wave energy.

Of course, this hypothesis is completely dependent on the timing of the draconic cycle agreeing with the empirical observation of QBO cycling. The predicted frequency for the multiplication of a draconic cycle convoluted with a semi-annual delta function impulse train is calculated as

365.25 modulo 27.2122 = 0.422 / year

or 2.368 years period due to physical aliasing of the waveforms (see Mathematical Geoenergy cited above). This indeed matches well the empirically observed cycling of QBO as shown in the time-series plot below, where all the excursions' pair one-to-one with observations, including potentially resolving the issue of the perturbation of 2016.

Responses: Following your comments here and our discussions through email, we performed the following four steps to realize aliased signals through the input-signals of annual cycle, lunar cycle, annual impulse.

First step: a semi-annual signal is constructed through the aliasing of an annual sinusoidal cycle and annual impulse. An artificial QBO signal is constructed through the aliasing of an lunar cycle and annual impulse. Here the dense sampling frequency is used.

An annual sinusoidal cycle is expressed as:

$$AO_{signal}(t_i) = A_{AO}\cos(2\pi t_i + \theta_{AO}). \quad (1)$$

Here A_{AO} and θ_{AO} are the amplitude and phase. The sampling frequency (F_{sampl}) is set to be 360 per year. The sampling time is $t_i = i/F_{sampl}$ and has unit of year. The index i is integer and is in the range of N years ($[0, N \cdot F_{sampl}]$). The sampling frequency is much higher than that used in the monthly QBO data and is used only for illustration purpose. Below, we will show that the sampling frequency can be set to be 12 (monthly data) for QBO signal. The black dots in Figure 1(a) shows the annual cycle in an interval of 16 years.

An annual impulse is expressed as a periodic Gaussian series ($x_i = t_i\%1$, % mean modulo):

$$AO_{impulse}(t_i) = \exp\left[-\frac{x_i^2}{2\sigma^2}\right] + \exp\left[-\frac{(x_i-1.0)^2}{2\sigma^2}\right] - \exp\left[-\frac{(x_i-0.5)^2}{2\sigma^2}\right]. \quad (2)$$

The series of annual impulse is shown as red dots in Figure 1(a).

Then, a semi-annual signal can be obtained through element-wise multiplication,

$$SAO_{signal}(t_i) = AO_{signal}(t_i) \times AO_{impulse}(t_i). \quad (3)$$

The $SAO_{signal}(t_i)$ is shown as black dots in Figure 1(b) and has clear semi-annual cycles.

In a same manner, we replace annual sinusoidal cycle with a lunar monthly sinusoidal wave with period of $\tau_L = 27.2122$ days to construct an artificial QBO signal. The lunar monthly sinusoidal wave is expressed as,

$$L_{signal}(t_i) = A_L \cos(2\pi F_L t_i + \theta_L). \quad (4)$$

Here A_L and θ_L are the amplitude and phase of lunar monthly sinusoidal wave. $F_L = \tau_Y/\tau_L$ is the frequency of lunar cycle with unit of cycles per year. The constant $\tau_Y = 365.2412384$ days is the period of one year corresponding to the sun's complete seasonal cycle. Now, an element-wise multiplication is performed on between $L_{signal}(t_i)$ and $AO_{impulse}(t_i)$. The multiplication result is shown as black dots in Figure 1(c) and exhibits an aliased ~2.3-year cycle.

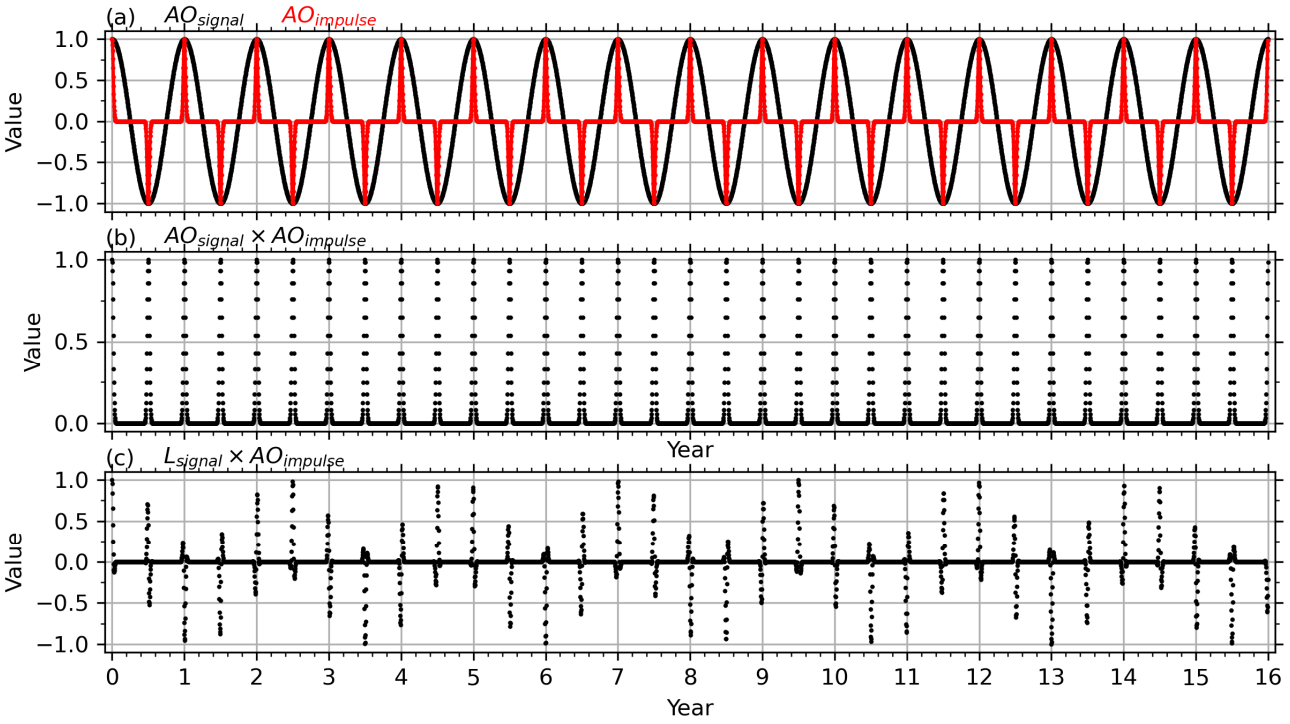

Figure 1: Temporal series of the annual sinusoidal cycle (AO_{signal}, black dots in a), annual impulse ($AO_{impulse}$, red dots in a), the resulted semi-annual cycle through multiplication between AO_{signal} and $AO_{impulse}$ (b), and the resulted QBO cycle through multiplication between L_{signal} and $AO_{impulse}$ (c).

Second step: an artificial QBO signal through a lunar cycle and annual impulse. Here the monthly sampling frequency is used. The "square off" QBO signal is obtained through the "sample-

and-hold" integration.

The dense sampling frequency in Figure 1 cannot be applicated to realistic QBO data, who has a sampling frequency of one month. Figure 2(a) shows the lunar monthly cycle with sampling frequencies of 360 per year (black, labeled with $L_{signal}(dense)$) and 12 per year (red, labeled with $L_{signal}(month)$). The lunar monthly cycle is accurately represented when the sampling frequency is 360 per year but is hard to be read. However, the lunar monthly cycle cannot be represented properly when the sampling frequency is 12 pers, which is lower than the minimum frequency required by the Nyquist sampling theory.

For the sampling frequency of 12 per year, the element-wise multiplication between $L_{signal}(month)$ and $AO_{impulse}$ (red in Figure 2b) results in signal with period of ~2.3-year (black dot in Figure 2b). The signal of ~2.3-year changes to be a "square off" temporal series (Figure 2c) after performing a special integrating process (i.e., sample-and-hold). The sample-and-hold integration means that a value of signal for that month is sampled, and then held constant until the next impulse, which is then added to the value.

It seems that the periodicity of the "square off" temporal series (Figure 2c) is more readable than the black dots series shown in Figure 2(b).

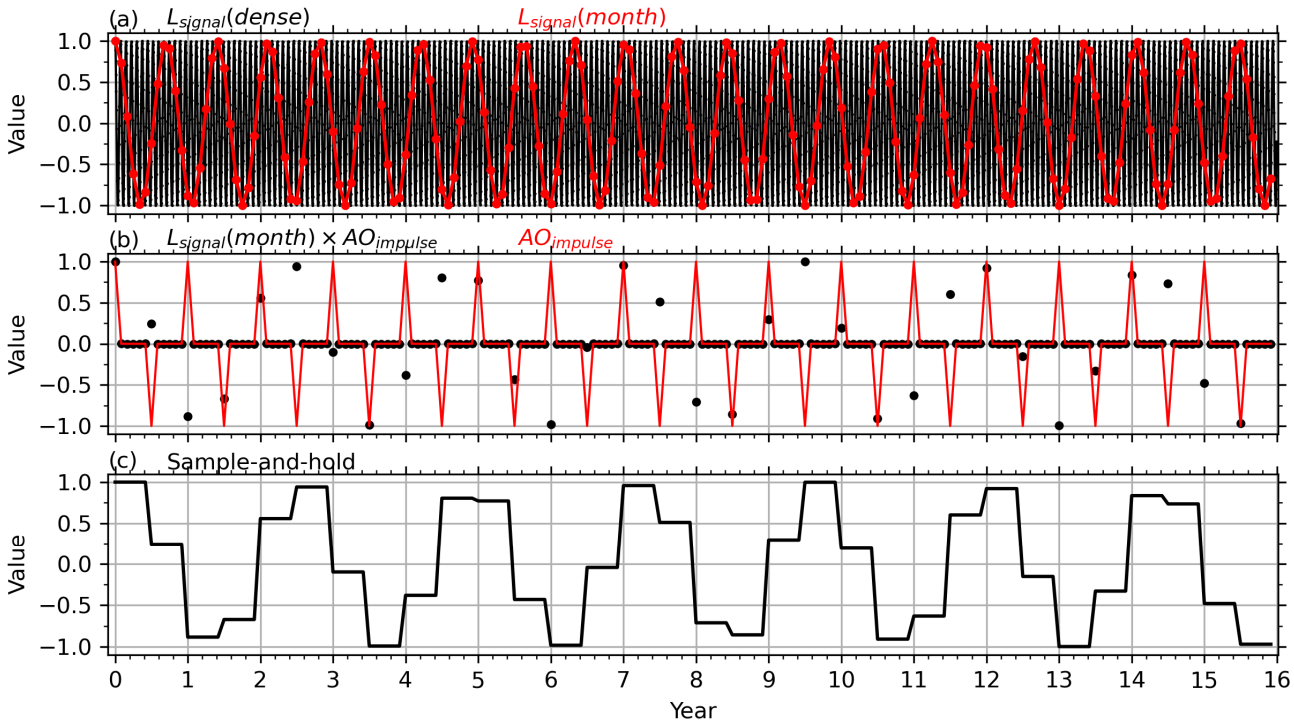

Figure 2: Temporal series of the lunar monthly sinusoidal cycles for the sampling frequency of 360 per year ($L_{signal}(dense)$, black in a) and 12 per year ($L_{signal}(month)$, red in a), annual impulse ($AO_{impulse}$, red in b) and the multiplication result (black in b), and the sample-and-hold integrating results (black in c) of the multiplication results shown as black dots in b.

Third step: the QBO signal is derived through aliasing of lunar cycle and seasonal cycles.

We follow the Equation 12.17-12.22 of the book edited by Pukite et al. (2019) to understand the modulo aliasing. The known lunar tidal forcing signal is periodic signal (i.e., Equation 4 and rewriting here):

$$L_{signal}(t_i) = A_L \cos(2\pi F_L t_i + \theta_L). \quad (5)$$

Here A_L and θ_L are the amplitude and phase of lunar monthly sinusoidal wave. $F_L = \tau_Y/\tau_L$ is the frequency of lunar cycle with unit of cycles per year. The constant $\tau_Y = 365.2412384$ days is the period of one year corresponding to the sun's complete seasonal cycle. The seasonal signal is likely a strong periodic delta function, which peaks at a specific time of the year. This can be approximated by a Fourier series of frequency i with unit of per year,

$$s(t) = \sum_{i=1}^{n} a_i \sin(2\pi t i + \theta_i). \quad (6)$$

Here, a_i and θ_i are, respectively, the amplitude and phase of the seasonal signal with frequency of i. Specifically, $i = 1$ corresponds to the annual cycle, $i = 2$ corresponds to the semi-annual cycle, etc.

The combination of the lunar cycle $L(t)$ amplified by a strongly cyclically peaked seasonal signal $s(t)$:

$$f(t) = s(t)L(t) = k \sum_{i=1}^{n} a_i \sin(2\pi f_L t + \phi) \sin(2\pi t i + \theta_i). \quad (7)$$

$$f(t) = \frac{k}{2} \sum_{i=1}^{n} a_i (\cos[2\pi(f_L - i)t + (\phi - \theta_i)] - \cos[2\pi(f_L + i)t + (\phi + \theta_i)]), \quad (8)$$

$$f(t) = \frac{k}{2} \sum_{i=1}^{n} a_i \cos[2\pi(f_L - i)t + (\phi - \theta_i)] - \frac{k}{2} \sum_{i=1}^{n} a_i \cos[2\pi(f_L + i)t + (\phi + \theta_i)]. \quad (9)$$

Equation (9) includes both the lower-frequency difference terms and higher-frequency additive terms. The lower-frequency terms are,

$$f_{LF}(t) = \frac{k}{2} \sum_{i=1}^{n} a_i \cos[2\pi f_i t + (\phi - \theta_i)]. \quad (10)$$

Here, $f_i = f_L - i$ is the frequency of difference aliasing, this can be used to construct the aliasing frequency listed in Table 11.1 of Pukite et al. (2019).

Table 1. The modulo aliasing frequencies and periods

Lunar frequency (f_L, 1/year)	Seasonal frequency (i, 1/year)	Frequency of difference aliasing (f_i, 1/year)	Period of difference aliasing (year)
13.422	10	3.422	0.292
13.422	11	2.422	0.412
13.422	12	1.422	0.703
13.422	13	0.422	2.368
13.422	14	-0.578	-1.730
13.422	15	-1.578	-0.634
13.422	16	-2.578	-0.388

Fourth step: Predictors used to reproduce the realistic QBO signal.

The predictors, which are used to fit the realistic QBO signal, can be constructed through aliasing of lunar cycle (cosine and sinusoidal form (Figure 3a)) and impulse with frequencies 10/12, 11/12, 12/12, 13/12, 14/12, 15/12, and 16/12 (red lines in Figures 3b-h). All predictors (black and blue in Figures 3b-h) have the "square off" form, which are obtained through element-wise multiplication of lunar cycle and impulse, and then through the "sample-and-hold" integration.

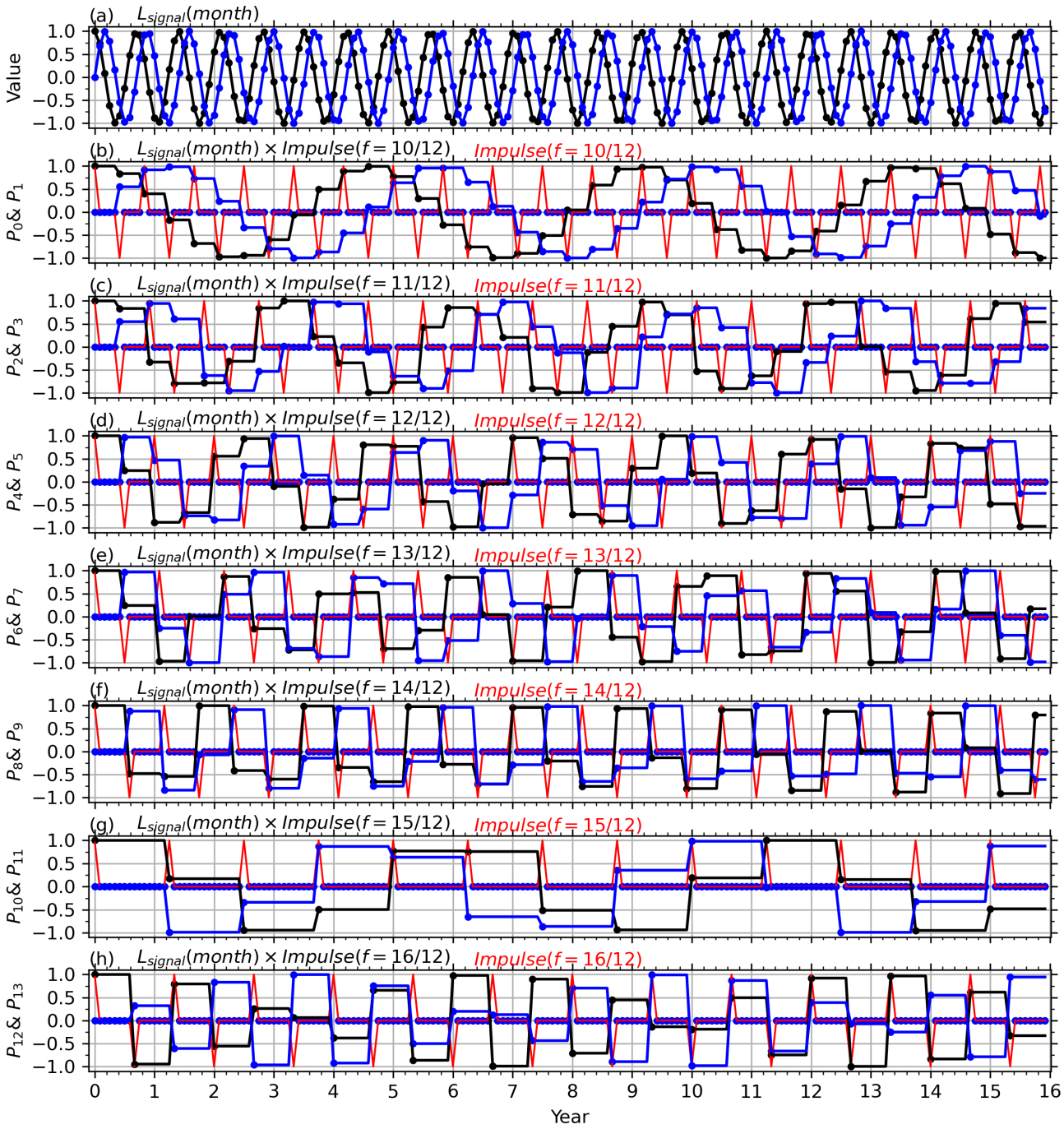

Figure 3: Lunar cycles in cosine (black in a) and sinusoidal form (blue in a) and predictors (black and blue in b-h).

Using the predictors shown in Figure 3, multiple linear regression (MLR) is used to fit the QBO wind at 30 hPa (black line in Figure 4a). The fitting and predicting results are shown as red line in Figure 4a. We note that the MLR model is trained in the interval of shaded region. The dominant contributions are the annual impulses (P_4 and P_5 in Figure 3d), that have largest regression coefficients. In a same manner, we show in Figure 5 the results of QBO wind at 10 hPa.

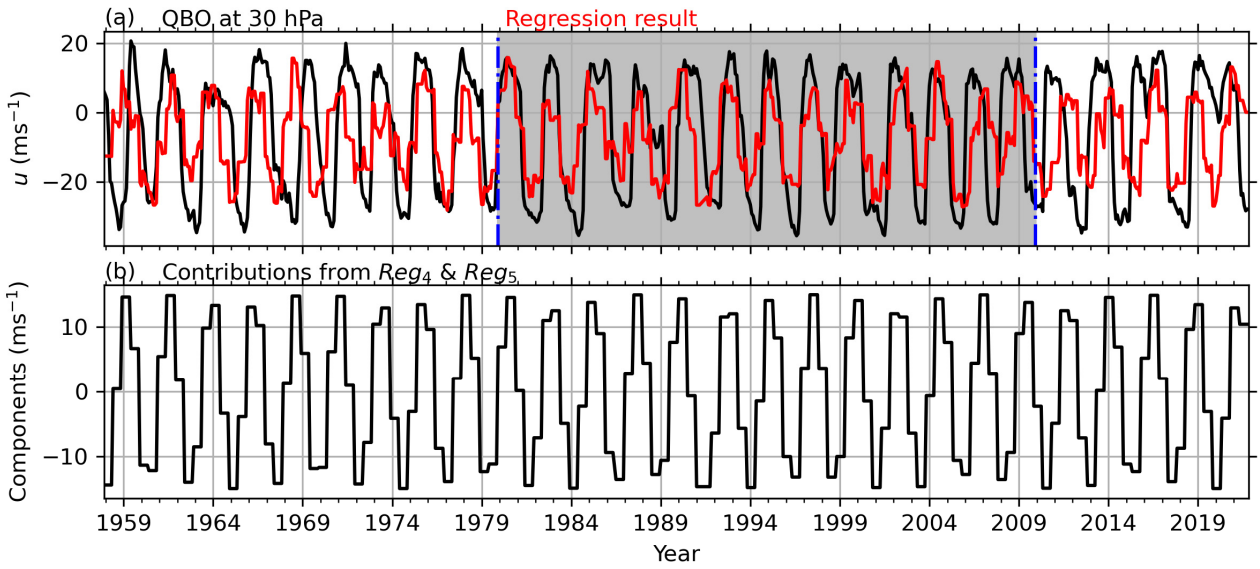

Figure 4: QBO wind at 30 hPa (black in a) and its MLR result (red in a). Also shown in b is the dominant contributions from the P_4 and P_5 in Figure 3(d).

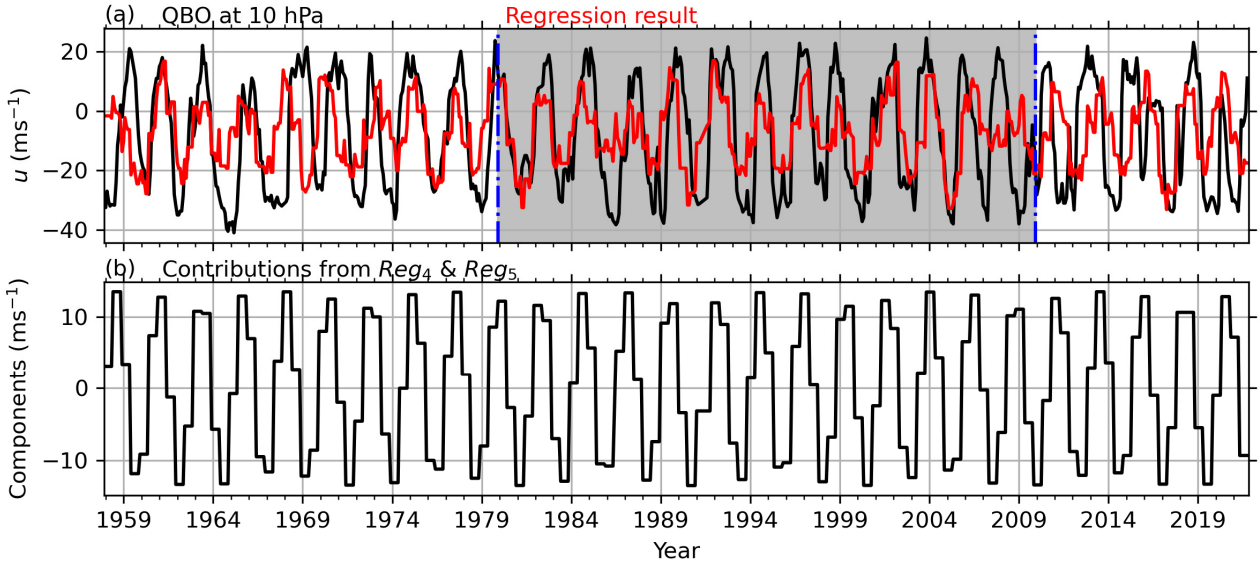

Figure 5: Same caption as Figure 4 but for the QBO wind at 10 hPa.

Using the aliased frequency shown in Table 1 and the sample-and-hold integration, Prof. Pukite has reproduced the QBO signal shown in Figure 5. This indicates that the lunar cycle, modulo aliasing with seasonal signal would generate an QBO signal.

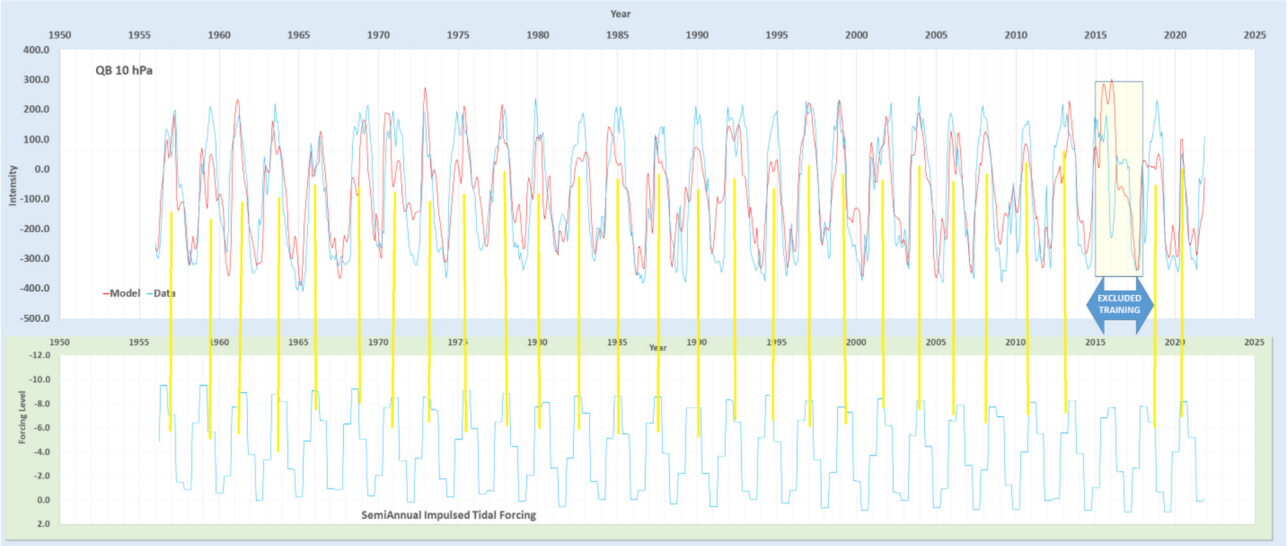

Figure 6: Provide by Prof. Paule R. Pukite, who reproduced QBO signal by using the aliased frequencies shown in Table 1 with variable initial phases.

Comparisons between Figures 5 and 6, we can see that fitting results by Prof. Pukite are better than those shown in Figure 5. This is because that Prof. Pukite included a gradient-descent algorithm to optimize correlation coefficient model fitting. The additional optimization improved the fitting to a higher quality.

The question as to why this correlation was missed by atmospheric scientists over the years is difficult to determine. Certainly, Richard Lindzen considered the possibility, as the cited quotes below reveal.

I can only offer again that conventional tidal analysis (for predicting king tides, etc.) operates at a local or regional level, where the 27.3216 days lunar synodic (or tropical) cycle is operational. For this particular lunar cycle, modulo arithmetic would generate an aliased ~2.7 years period, which is not close enough to match the long-term QBO periodicity observed. Yet, for conventional tidal analysis, the draconic tidal factor never appears in any analyses, since globally synchronized tides would never be considered, and also importantly, the modulo arithmetic of impulse driven signals at the edge of metastability is also not applied. This means that two critical assumptions – (1) nodal lunar cycling and (2) modulo aliasing – need to be considered, which in retrospect could have easily been overlooked as together they are a necessary condition. A third assumption, that solutions of Laplace's Tidal Equations as applied to the equatorial waveguide can provide the non-linear shaping to allow model fitting to the family of QBO time-series is also described in Mathematical Geoenergy.

"For oscillations of tidal periods the nature of the forcing is clear"
Lindzen, R. D. (1967). Planetary waves on beta planes. Monthly Weather Review, 95(7), 441–

451

“It is unlikely that lunar periods could be produced by anything other than the lunar tidal potential”

Lindzen, R. S., & Hong, S.-S. (1974). Effects of mean winds and horizontal temperature gradients on solar and lunar semidiurnal tides in the atmosphere. Journal of the Atmospheric Sciences, 31(5), 1421–1446.

The intention of this comment is to provide alternative explanations via geophysics. A tidal approach is much more plausible and parsimonious than attempting to apply variations in solar output via sunspot activity, which the authors of the paper under review consider. The elegance of transitioning from the semi-annual oscillation of the upper stratosphere to the lunar-modified oscillation of the denser lower density cannot be easily refuted. If Lindzen had the insight to realize the connection in the late 1960’s much more effort could have been applied to model the behavior and apply it to other aspects of climate.

Responses: Your comments are valuable for us to understand the mechanism of QBO in the lower stratosphere. We believe that you provide a new insight on this point, which has been added in the Introduction as “Recently, Pukite et al. (2018) proposed that the QBO signal in the stratosphere can be generated by the modulo aliasing between nodal lunar cycle (27.2122 days) and seasonal impulse signals. Especially, the modulo aliasing between the lunar cycle and an annual impulse results in a signal with periods of 2.3 years, which is close the QBO periods of 2–3 years”.